Нови материјали

New materials in electrical and electronic engineering

Raman spectra of the materials based on mechanically activated alkaline earth metal titanates

Vera P. Pavlović, Ani Tshantshapanyan, Branislav Vlahović, Jelena Živojinović, Darko Kosanović, Vladimir B. Pavlović

***Abstract* — The changes in the Raman spectra of electronic materials obtained from mechanically activated $BaTiO_3$ and $SrTiO_3$ powders, with or without additives, are presented in this paper. Mechanical activation, performed in a high-energy planetary ball mill, was chosen as the method for the production of fine-grained nanocrystalline powders with an increased surface activity and an altered micro and/or crystal structure. Having in mind the growing relevance of the development of multiferroic materials, the analysis of Raman spectra was used not only for the structural investigations of the mechanically activated undoped titanate powder, but also for the examination of the mechanically activated Fe/$BaTiO_3$ system and the subsequent hexaferrite formation during the sintering process. Additionally, Raman spectroscopy was applied in the study of the emergence of electroactive crystalline phases in nanocomposites based on semi-crystalline fluoropolymers, such as PVDF (polyvinylidene fluoride), in the case when mechanically activated $BaTiO_3$ powder was used as a filler in the polymer matrix. Furthermore, the effects of the mechanical activation of $SrTiO_3$ powder on the occurrence of polar nano and micro-regions at room temperature, as well as the simultaneous influence of activation and MnO_2 addition on structural changes in ceramic $SrTiO_3$ samples, have also been analysed using Raman spectroscopy.**

***Index Terms* — Raman spectroscopy, mechanical activation, $BaTiO_3$, $SrTiO_3$, nanocomposites, multiferroics.**

I. Introduction

Raman spectroscopy is primarily a vibrational spectroscopic method, used for non-destructive characterization of materials. It provides information on the vibrational spectra of molecules, which can be used to identify certain compounds, crystal modifications or functional groups, as well as to trace some structural changes [1, 2]. The method is often considered to be complementary to IR spectroscopy and is widely used as an additional investigation procedure to XRD and other structural analyses. The principle of Raman spectroscopy relies on the inelastic scattering of monochromatic light on the crystal lattice of the investigated sample. The term *Raman spectroscopy* primarily refers to the scattering of photons by phonons [3]. The so-called Raman shift, which is the difference in the wave number of incident and scattered radiation, is the main parameter analyzed in Raman spectroscopy, because this difference directly depends on the type of molecules, molecular groups and certain crystal modifications, as well as in general on the structure of the tested sample.

$BaTiO_3$ and $SrTiO_3$ belong to the group of alkaline earth metal titanates usually considered to be model perovskite materials, i.e. easily functionalizable materials that are intensively and widely applied in electronics. Barium titanate has been the most extensively investigated lead-free ferroelectric material, with a high dielectric constant, widely utilized to manufacture electronic components. Most applications of barium titanate-based materials include the production of multilayer capacitors (MLCs), piezoelectric devices, positive temperature coefficient thermistors, high-density optical data storage, communication filters and nonvolatile memories, etc. [4]. Along with being used as sensors and multilayer ceramic capacitors (MLCCs), materials based on strontium titanate are also used as catalysis, in UV detectors and solar cells, in DRAMs and energy storage devices, etc. [5]. Due to the persisting need to miniaturize electronic devices, it is necessary to obtain smaller and more uniform particle sizes of electronic materials. Among numerous methods for the production of $BaTiO_3$ and $SrTiO_3$ fine powders, such as the sol–gel synthesis, oxalate process, hydrothermal synthesis, the combustion of a dehydrated form of the precursor complex, polymeric precursor and solvothermal methods, etc., mechanical activation has been identified as a very effective and low-cost method for obtaining a highly dispersed system, enabling the directed modification of the structure and properties of activated material. Barium titanate ceramics obtained from mechanically activated powders may have a higher piezoelectric coefficient, as well as modified values of

Vera P. Pavlović is with the University of Belgrade, Faculty of Mechanical Engineering, Kraljice Marije 16, 11120 Belgrade, Serbia (e-mail: vpavlovic@mas.bg.ac.rs).

Ani Tshantshapanyan is with the North Carolina Central University, 18001 Fayetteville Street, Durham, NC 27707, USA (e-mail: atshants@nccu.edu)

Branislav Vlahović is with the North Carolina Central University, 18001 Fayetteville Street, Durham, NC 27707, USA (e-mail: vlahovic@nccu.edu).

Jelena Živojinović is with the Institute of Technical Sciences of the Serbian Academy of Sciences and Arts, Knez Mihailova 35, 11000 Belgrade, Serbia (e-mail: jelena.zivojinovic@itn.sanu.ac.rs)

Darko Kosanović is with the Institute of Technical Sciences of the Serbian Academy of Sciences and Arts, Knez Mihailova 35, 11000 Belgrade, Serbia (e-mail: darko.kosanovic@itn.sanu.ac.rs)

Vladimir B. Pavlović is with the Institute of Technical Sciences of the Serbian Academy of Sciences and Arts, Knez Mihailova 35, 11000 Belgrade, Serbia (e-mail: vladimir.pavlovic@itn.sanu.ac.rs).

dielectric permittivity, a lower Curie point and a flattened curve of $\varepsilon_r = f(T)$ dependence, which are the effects analogue to those obtained by adding various additives such as $SrTiO_3$, $BaZrO_3$ and $SnTiO_3$, or $CaTiO_3$ and $MgTiO_3$ [6]. On the other hand, the mechanical activation of $SrTiO_3$ may influence not only its dielectric properties, but also its optical properties and electrical conductivity, regarding the increase in the concentration of defects such as oxygen vacancies.

The utilization of $BaTiO_3$ and $SrTiO_3$ materials as fillers within a polymer matrix in the production of composite materials with improved electroactive properties is also an increasingly interesting topic. Among the various polymers that can be used for these purposes, PVDF has been identified as a semi-crystalline fluoro-polymer which has polar crystalline phases, such as beta and gamma crystal modifications, along with non-polar ones. The ferroelectric and piezoelectric properties of PVDF are determined by the presence of these polar phases, especially the beta phase. It is noteworthy that PVDF, as well as the composites based on it, has some advantages over purely ceramic ferroelectric samples, since PVDF is marked by low density, high flexibility, sufficient strength, toughness and the ability to be easily produced in a technologically useful form [7]. It is generally recognized that PVDF and its co-polymers have a huge potential as dielectric materials, especially in those applications where high-energy density and low loss at high repetition rates are required [8].

It has been found that $BaTiO_3$-based materials can simultaneously exhibit ferroelectricity and ferromagnetism at room temperature, depending on the type and concentration of the dopant. According to the literature data, the incorporation of 3d and 4d transition metals as a substitute for the titanium atom in barium titanate may produce ferromagnetism, inducing multiferroicity. For instance, room-temperature ferromagnetism has been reported in Mn-, Fe- and Co-doped $BaTiO_3$ systems. It has been observed that the substitution of Fe at the B-site improves the coercive field, while the substitution at the A-site increases saturation magnetization [9]. Besides, barium hexaferrite $BaFe_{12}O_{19}$ (often denoted as BaM) and Fe-ion substituted ferrite materials based on it have been extensively used due to their multiferroic properties. Barium hexaferrite belongs to the M-type hexaferrites, which are based on a hexagonal "magnetoplumbite" or M-structure. This symmetry belongs to the space group $P6_3/mmc$ with 64 atoms in a unit cell [10]. BaM is marked by large spontaneous polarization at room temperature, a clear ferroelectric hysteresis loop, high saturation magnetization, high intrinsic coercivity (for both ferroelectric and magnetic hysteresis) and high ferrimagnetic transition temperature. These features make it suitable for application, especially if we keep in mind that it is possible to control both polarization and magnetization via an external electric and/or magnetic field [11]. The large uniaxial anisotropy can be overcome by substituting a Fe^{3+} ion (e.g. with Co^{2+} and Ti^{4+}), which endows ferrite with an excellent soft magnetic property with a high magnetic permeability [12]. BaM has found wide applications in technology as a permanent magnet, in microwave devices, sensors, particulate perpendicular high-density recording media, high-frequency circuits and in many other magnetically operated devices [10]. However, the production of pure or substituted BaM is normally accompanied with the presence of residual nonmagnetic phases, such as hematite (α-Fe_2O_3), which can be associated with the choice of the Fe:Ba molar ratio in the starting powder. Therefore, an extensive research has been carried out to synthesize M-type hexaferrites from starting powders with an off-stoichiometric Fe:Ba ratio.

Doping $SrTiO_3$ with transition metals such as Mn is also interesting, not only with the aim of introducing ferromagnetic behavior and the coexistence of a glassy magnetic state and a glassy dielectric behavior in a Mn-doped $SrTiO_3$ system, but also to modify and tune dielectric permittivity and dielectric loss, which depends on the site of ion incorporation in the lattice (at the Sr or Ti site) [13]. To the best of our knowledge, there are no reports on the simultaneous effect of Mn-doping and mechanical activation of strontium titanate on its structure and properties.

This paper presents an overview of the application of nonresonant Raman spectroscopy in the analysis of structural changes in materials obtained from mechanically activated $BaTiO_3$ and $SrTiO_3$ powders. Having in mind the importance of obtaining light, flexible and easily processed electroactive nanocomposite films for the application in the production of pressure and IR sensors etc., structural changes in polymer composite films with a mechanically activated titanate as a filler were also analyzed using Raman spectroscopy. The Raman analysis of a mechanically activated Fe/$BaTiO_3$ system and hexaferrite $BaTi_xFe_{12-x}O_{19}$ synthesized from this system is presented as well, including the investigation of the influence of laser power on the obtained results. The application of Raman spectroscopy in the assessment of the dopant incorporation into the $SrTiO_3$ lattice was additionally considered.

II. Materials and Methods

Commercially available $BaTiO_3$ powder (Aldrich, p.a. 99.9%) was mechanically activated in a planetary ball mill (Fritsch Pulverissete), up to 60 minutes, and an analogue procedure was applied for $SrTiO_3$ (99% purity, mean particle size ≤ 5 μm). The X-ray powder diffraction patterns of the initial and activated powders were obtained using $CuK_{\alpha 1/2}$ filtered radiation. The Raman scattering of the samples was recorded at room temperature, in a backscattering geometry, using the 514.5 nm line of an Ar^+ ion laser for the $BaTiO_3$ spectra, and the 633 nm line of a He-Ne laser for the $SrTiO_3$ spectra. The $BaTiO_3$ that had been mechanically activated for a short period of time was used as a filler in the PVDF (polyvinylidene fluoride) matrix. The Raman spectra of these systems were taken by applying a He-Ne laser. Nanocomposite films were prepared by the solution casting method. In order to obtain the $Sr_{1-x}Mn_xTiO_3$ or $SrTi_{1-x}Mn_xO_3$ system, where x=0.03, x=0.06 and x=0.12, MnO_2 was added to the starting $SrTiO_3$ powder. The powders were

mechanically activated for 10, 30 and 120 min, under the same conditions as for pure $SrTiO_3$, but with the addition of ethanol. After the activation, the samples were dried at 100 °C for 3.5 h and sintered at 1200 °C. The Raman examination of the influence of mechanical activation and doping was performed using the 532 nm line of the Nd:YAG laser. The mixture of commercially available Fe and $BaTiO_3$ powders (weight % ratio: 60:40) was also mechanically activated up to 240 minutes in a planetary ball mill, calcined at 700 °C for 2 h and sintered at 1200 °C, in order to obtain hexaferrite ceramics. The influence of mechanical activation on the Raman spectra of the calcined mixture and sintered samples was monitored using the 633 nm line of a He-Ne laser. Two different laser beam power values were applied on the sample.

III. Main Results

A. *Raman spectra of mechanically activated barium titanate*

The role of Raman spectroscopy in the assessment of the dominant crystal modification and in the monitoring of the trend of structural changes in mechanically activated $BaTiO_3$ was analysed as the first example. It is known that size effects can influence the stability of the $BaTiO_3$ ferroelectric phase at room temperature, leading to the occurrence of the cubic phase [14]. The critical size below which the $BaTiO_3$ crystal structure changes from the tetragonal (ferroelectric) to the cubic phase usually varies from 20 to 100 nm, depending on the processing route [15]. Mechanical activation can generally lead to significantly reduced mean particle and crystallites sizes, which is usually accompanied with an increased value of microstrains. The formation of uncompensated stress during mechanical activation also causes tetragonal distortion, which can be manifested as the change in crystal lattice parameters [16, 17]. All these effects cause both the broadening of diffraction lines and the decrease in their integral intensity, making the assessment of the crystal structure type much more difficult (Fig. 1).

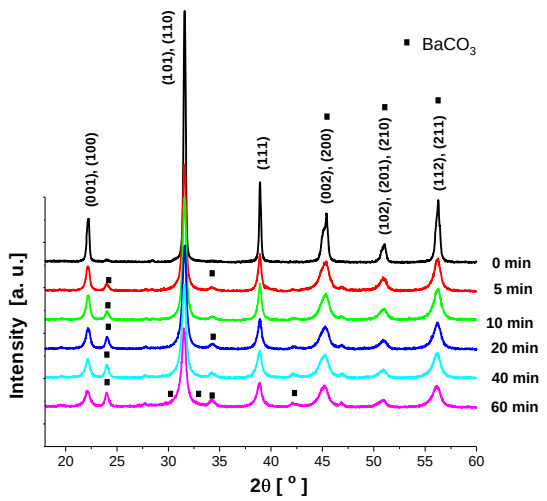

Fig. 1. XRD spectra of mechanically activated barium titanate.

Generally, the XRD peak in the range $2\theta \in (44 - 46)^o$ is especially important in estimating the presence of the cubic or tetragonal crystal modification of $BaTiO_3$. Namely, in a typical tetragonal structure with micron-sized crystallites, the mentioned peak occurs as a doublet (002, 200), with a clearly expressed split of the peak into two components. On the other hand, in a typical cubic structure there is no splitting and the peak is completely symmetrical. However, in case of a slightly sustained tetragonal or pseudocubic structure in $BaTiO_3$, where the mean crystallite size is on the scale of 100 nm or less, only the weak peak asymmetry instead of splitting may be observed, due to the broadening, shifting and overlapping of diffraction lines [14]. Therefore, in fine-grained and nanocrystalline $BaTiO_3$ careful additional comparison between the widths of the doublet and a singlet is required, as well as a very careful Rietveld refinement of the whole diffractogram. In such cases, it is especially important to obtain information about the present crystal modifications on the basis of other nondestructive methods, such as Raman spectroscopy. Although the tetragonal $BaTiO_3$ has eight Raman active modes (three A_1, one B_1 and four E modes) according to theoretical selection rules, the effects like the overlapping of some modes (A_1 and E, or B_1 and E) and the existence of a coupled-mode interaction, as well as the overdamped character of the lowest optical E mode (E(1TO) soft mode), commonly lead to a smaller number of Raman peaks in the experimentally obtained unpolarized spectrum of polycrystalline samples. It can be seen in Fig. 2 that all experimentally expected Raman peaks, typical for microcrystalline $BaTiO_3$ powders and ceramics [18,19], are found in the spectrum of the nonactivated sample.

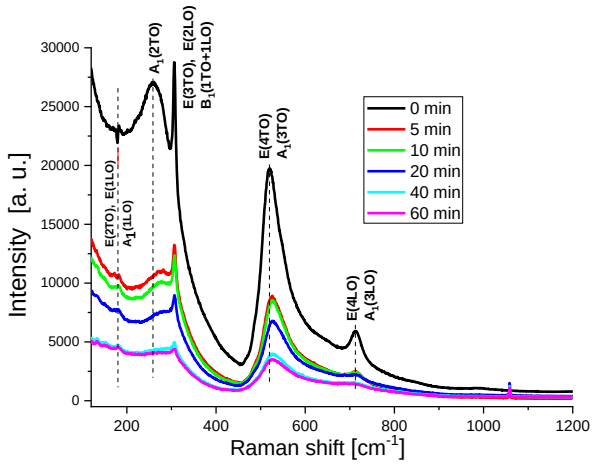

Fig. 2. Raman spectra of mechanically activated barium titanate.

It is demonstrated that a diminution in particle and crystallite size during mechanical activation lasting up to 60 minutes, as well as an increased concentration of defects and the disorder induced in the $BaTiO_3$ powders activated for longer periods, lead to decreased peak intensities, accompanied with their gradual broadening. The sharpest peak, known as typical of the tetragonal $BaTiO_3$ structure, decreases as well in the

obtained spectra, but remains sufficiently noticeable even for prolonged activation times, indicating posible domination of the tetragonal structure in the nanocrystaline powder, although with a slightly sustained tetragonality. This example illustrates the importance of Raman spectroscopy application in assessing the presence of the tetragonal crystal modification in the perovskite structure, especially when particle and crystallite sizes in the material are sufficiently small to cause a prominent broadening and the overlapping of the XRD lines essential for the polymorph phase discrimination. The conclusions derived based on Raman spectroscopy may be very helpful in the Rietveld analysis of XRD spectra. In this case, the Rietveld analysis of the X-ray diffraction patterns of mechanically activated $BaTiO_3$, correlated with the observations from the Raman spectra, shows that mechanical activation for up to 60 minutes lead to a significant reduction of the mean crystallite size from 150 nm to ~ 30 nm [20], but the tetragonal structure persist as the dominant. The deconvolution of the Raman spectra may reveal important parameters, such as the positions of the modes and the relative change of the FWHM values (Fig. 3).

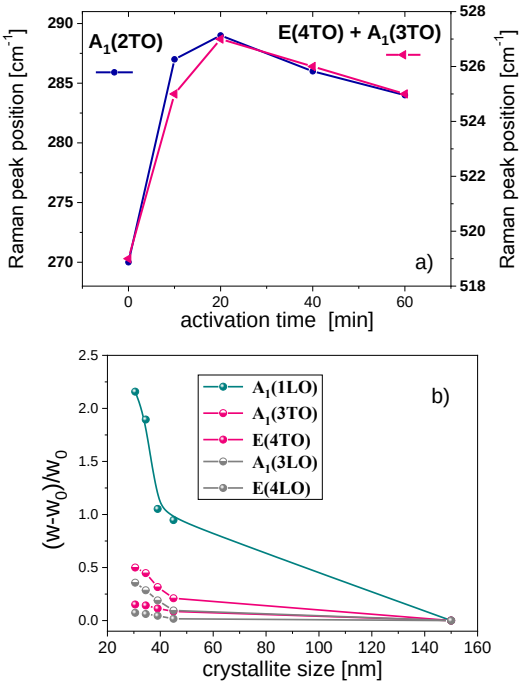

Fig. 3. a) The influence of activation time on the position of those Raman peaks which include A_1(TO) modes; b) Relative change of the FWHM for modes assigned to Raman peaks at ~180, 520 and 720 cm^{-1}, versus crystallite size.

In case of mechanically activated $BaTiO_3$, the significant blue shift of the two main broad Raman peaks observed in the range up to 600 cm^{-1} (Fig. 3a) confirms that the A_1(TO) modes are sensitive to impurities or structural defects, although the mentioned shift could also be attributed to mechanically introduced stress effects, primarily to an increased tensile stress [21]. Some of the low-intensity bands in the region under 170 cm^{-1} are detected in the samples activated for longer periods (Fig. 2), indicating changes in the vibrations of Ti and TiO_6 octahedra, due to the formation of oxygen and/or barium vacancies and other $BaTiO_3$ intrinsic structural defects [22].

B. Raman spectra of PVDF polymer and PVDF-based nanocrystalline composites

Raman spectroscopy was also applied for the assessment of the type of the dominant crystal modification of the low-density fluoro-polymer PVDF matrix, after the incorporation of mechanically activated $BaTiO_3$ as a filler [23]. It is known that PVDF is a semi-crystalline fluoro-polymer, which can crystallize in several modifications. Although theoretically five crystal modifications may occur, some of the following three phases are usually present: alpha, beta and gamma. The alpha phase is the most common, but electroactive phases such as beta and gamma are important for application in electrical components. Only the β-phase is suitable for most sensor applications, since it has the most pronounced ferro-, piezo- and pyroelectric properties, due to larger spontaneous polarization [24, 25]. For these reasons, intensive research efforts towards obtaining PVDF films with the largest possible share of the beta phase are of key interest. Since some of the strongest XRD lines of the three common PVDF crystal phases (α, β and γ) are very close to each other and they partially overlap, the investigation of Raman spectra may be crucial for the conclusions regarding the present phases. The broad-ranged Raman spectra of polymers are very complex to analyze, not only due to the multitude of peaks belonging to the polymer and the filler, but also because of the frequent emergence of fluorescence, which raises the background signal, thereby reducing the observable intensity of the diffraction lines belonging to crystal phases. The part of the entire recorded Raman spectrum of the PVDF-based composites that is the most relevant for the identification of crystalline phases in the PVDF polymer and the PVDF-based composites is presented in Fig. 4.

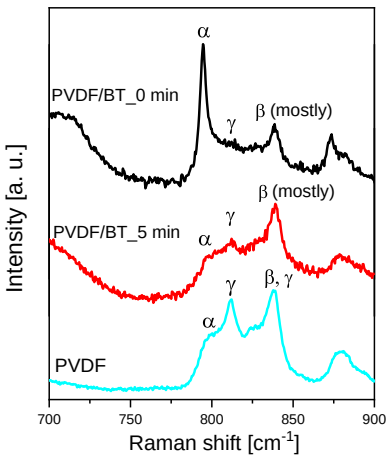

Fig. 4. The enlarged part of Raman spectra of PVDF and PVDF-based composites with non-activated and activated $BaTiO_3$ as a filler.

Fig. 4 shows how the incorporation of the nonactivated and shortly activated $BaTiO_3$ powder into the PVDF matrix changes the share of crystalline phases in the polymer, i.e. in the composite. It can be observed that the gamma phase dominates in the analyzed pure PVDF polymer, because the peak at 812 cm^{-1} is clearly expressed only when the gamma phase is dominant [26]. The injection of the nonactivated $BaTiO_3$ powder, with a weight fraction of 2%, enhances the domination of the alpha phase, while the injection of the same amount of the $BaTiO_3$ powder activated for 5 minutes promotes the formation of the beta phase, which becomes dominant. This was probably caused by the smaller particle sizes, a larger specific surface area and consequently higher surface activity of the mechanically activated powder. Namely, these modifications were detected in the $BaTiO_3$ powder activated for a short period using SEM method and mercury porosity [27]. Such modifications of the filler particles may amplify the interaction between the filler and the polymer, promoting the conformation of the polymer chains corresponding to the beta crystalline phase of PVDF. The share of the beta phase in the activated filler is significantly larger than the share of the gamma phase, while the formation of the alpha phase is suppressed. This is an important effect, since the beta phase of PVDF has the most pronounced ferroelectric properties, while the nanocrystalline filler activated for a short period keeps the tetragonal (ferroelectric) structure almost unchanged.

C. Raman spectra of Fe/$BaTiO_3$ system and hexaferrite

In the previous sections, the examples of Raman analyses of a one-component system ($BaTiO_3$ powder) and a two-component PVDF/BT system were discussed. In the latter case we can even speak of a multi-component system, if we consider the number of the crystalline modifications of PVDF. Having in mind the increasing importance of the development of multiferroic materials, we will present the application of Raman analyses for the examination of the mechanically activated Fe/$BaTiO_3$ system and the subsequent hexaferrite formation during the sintering process, in the following passages. A mixture of Fe and $BaTiO_3$ powders (weight percent ratio: 60:40) was mechanically activated up to 240 minutes in a planetary ball mill and calcined at 700 ^{o}C for 2 h. The phase composition was investigated by means of the XRD and Raman methods. Since Raman spectroscopy cannot be used to detect pure metal modes, there are no modes in the Raman spectrum that corresponded to iron, while the diffraction patterns show distinct Fe peaks for all activation times [28]. The dependency of the obtained Raman spectra on both time of mechanical activation and the laser beam power at the sample was studied. The Raman spectra recorded under the lower power at the sample (0.6 mW) show that the mechanical activation longer than 100 minutes promotes the formation of hematite during the activation and leads to the formation of other iron-oxide phases, such as magnetite and wustite (Fig. 5). The Raman spectrum of the sample corresponding to the longest activation time reveals the domination of iron oxide. The hematite mode corresponding to the second order scattering also appears. These results are completely consistent with the obtained XRD spectrum [28]. After correlating the lower- and higher-power Raman spectra with the XRD results, it has been concluded that the increase in the beam power at the sample up to 1.2 mW changes the phase ratio in the sample, i.e. causes an enhanced phase transition from magnetite to hematite (Fig. 6).

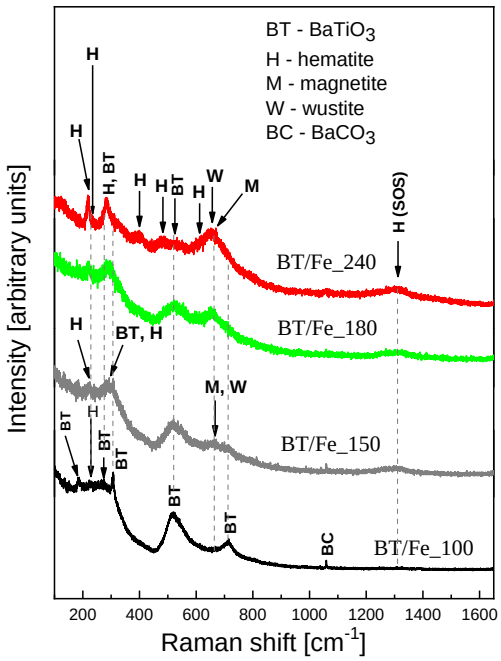

Fig. 5. Raman spectra of mechanically activated mixture of Fe and $BaTiO_3$ powders (the power of a laser beam at the sample: 0.6 mW).

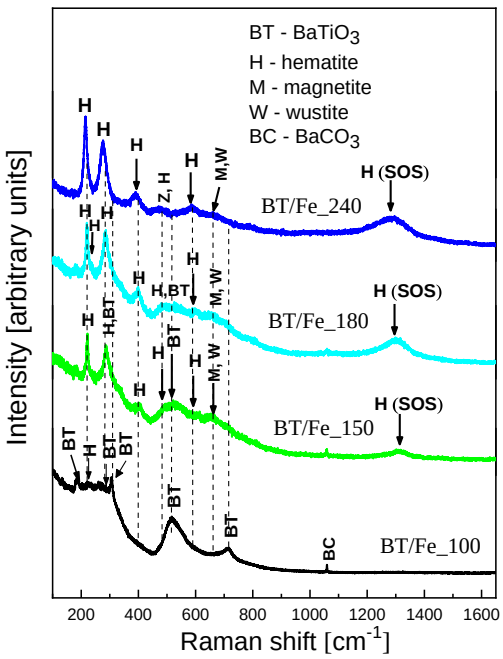

Fig. 6. Raman spectra of mechanically activated mixture of Fe and $BaTiO_3$ powders (the power of a laser beam at the sample: 1.2 mW).

It has also been observed that mechanical activation decreases the temperature of the phase transition from wustite to magnetite and from magnetite to hematite. This effect emphasizes that in Raman spectroscopy the laser power on the sample does not only affect the signal strength, but can cause a local increase in temperature that is sufficient to give rise to some phase transitions in certain systems such as iron oxide, thus significantly changing the spectrum. Although our higher laser power value was still in the range where no phase transition from one iron-oxide phase to another was expected in the nonactivated sample, mechanical activation changed the upper limit of the mentioned range. Based on the literature data about the influence of laser power on phase transition in nonactivated magnetite [29], we can conclude that the transition from magnetite to hematite takes place at a much lower power in the mechanically activated samples, than in nonactivated magnetite.

The calcined samples were sintered at 1200 °C, in order to obtain hexaferrite. The Raman spectra of the sintered samples are shown in Fig. 7. Both XRD and Raman analyses indisputably show that hexaferrite (pure or cation-substituted) was formed in all samples (for all activation times) and that hexaferrite modes were dominant [30].

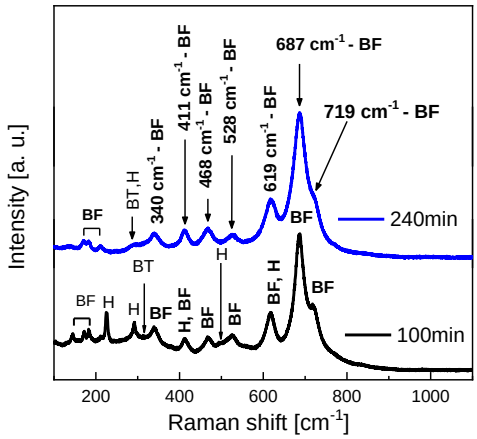

Fig. 7. Raman spectra of ceramics obtained from mechanically activated Fe/$BaTiO_3$ system (BF – barium hexaferrite, BT – $BaTiO_3$, H – hematite).

Weak modes of residual hematite and $BaTiO_3$ are also observed in the spectrum. The number and intensity of these modes decrease with prolonged mechanical activation, as expected. However, it should be noticed that the Raman spectra presented in Fig. 7 do not indicate an unambiguous conclusion regarding the formula of hexaferrite. The XRD analysis suggests that Ti-substituted BaM was obtained, i.e. $BaTi_xFe_{12-x}O_{19}$, which could be expected based on the starting components. Namely, the Ritveld analysis (the refinement of the entire diffraction profile, the determination of the occupation numbers, etc.), indicates that the formula of the obtained hexaferrite is: $BaFe_{11.23}O_{19}Ti_{0.77}$. Yet, according to the literature data [10, 31] our Raman spectra have the characteristics of both compounds – pure BaM and Ti-substituted hexaferrite, which makes an estimation of the parameter x more difficult. The reason for the highlighted ambiguity lies in the fact that barium hexaferrite belongs to very complex systems. It has 64 ions per unit cell, on 11 different symmetry sites, where 24 Fe^{3+} ions are distributed over five different symmetry sites: three kinds of octahedral sites, one tetrahedral site and one bipyramidal site [10]. Although Raman spectroscopy can be used to study the distribution of cations in a system, the assessment is usually sufficiently accurate in less complicated systems. In addition, despite the widespread application of the BaM system, it is still impossible to find a sufficiently complete database for its Raman spectra, and the existing spectra of BaM and Ti-substituted BaM sometimes seem contradictory, both in terms of peak shapes and peak positions. Therefore, it is of great interest to enrich the existing databases with the Raman spectra of pure and cation-substituted barium hexaferrite obtained via different procedures.

D. Raman spectra of mechanically activated undoped and Mn-doped $SrTiO_3$

The analysis of the Raman spectra of the mechanically activated $SrTiO_3$ reveales that along with the dominant second-order scattering several very weak first-order Raman modes occur (Fig. 8) due to imperfections in the $SrTiO_3$ cubic structure at room temperature. While the intensity of second-order peaks decreases with the longer activation times, the intensity of the polar modes TO_2 and TO_4 increases. The modes X_1 and X_2 show simmilar dependance. According to the literature data, the shape and the intensity of polar TO modes in $SrTiO_3$ may significantly depend on defects such as oxygen vacations [32].

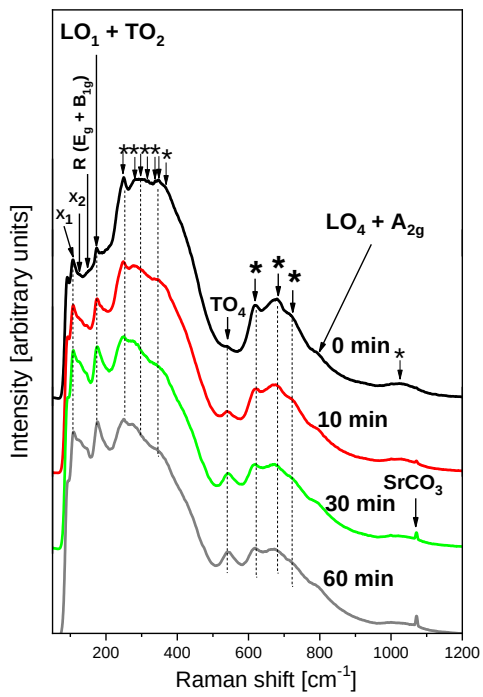

Fig. 8. Raman spectra of mechanically activated strontium titanate.

The characteristic Fano shape of the TO_2 Raman line suggests a high probability of the presence of polar micro- and nanoregions (which coexist with the dominant paraelectric phase) in the activated $SrTiO_3$. A considerable increase in the TO_4 mode intensity (Fig. 8) supports this assumption as well. It is accepted in the literature that the TO_2 mode intensity is proportional to the total volume of polar microregions, and that the occurrence of TO_2 mode may be accompanied with the remnant polarization [33]. However, the silent mode remains unnoticeable in the activated samples, indicating that the long-range structural distortion has not been established, as well as that the number of polar micro-regions is small and there is still no overlap between the adjacent polar micro-regions. The performed Raman spectroscopy gives clear evidence about the blue shift of the TO_4 mode, X_1 mode and (LO_1+TO_2) doublet (Fig. 8), which is primarily a result of the introduction of microstress into the $SrTiO_3$ lattice, but also a consequence of the reduced crystallite sizes.

Additional investigations were performed in order to apply Raman spectroscopy for monitoring the influence of mechanical activation on incorporation of the Mn ions into the $SrTiO_3$ lattice. In order to obtain a $Sr_{1-x}Mn_xTiO_3$ or $SrTi_{1-x}Mn_xO_3$ system, where x=0.03, x=0.06 and x=0.12, MnO_2 was added to the starting $SrTiO_3$ powder. The powders were mechanically activated for 10, 30 and 120 minutes, under the same conditions as for a pure $SrTiO_3$, but with the addition of ethanol. After activation, the samples were dried at 100 ^oC for 3.5 h and sintered at 1200 ^oC. The spectra of the nonactivated samples and of the samples activated for 120 min are shown in Fig. 9, which includes undoped and differently doped samples.

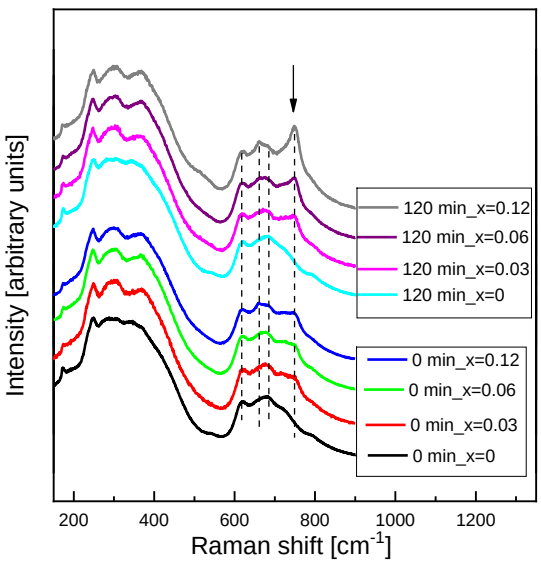

Fig. 9. Raman spectra of Mn-doped $SrTiO_3$ ceramics.

Fig. 9 shows that the peaks obtained as a result of the second order scattering are generally more distinct in doped samples, especially in the Raman shift range above 720 cm^{-1}. Actually, in those samples the occurrence of the peak at ~750 cm^{-1} is observed, whereby its intensity increases with increased dopant concentration. The influence of the changes in the manganese concentration on the high-frequency part of the broad second-order Raman effect in the Raman shift region above 590 cm^{-1}, in the Sr_{1-x} Mn_xTiO_3 and $SrTi_{1-x}Mn_xO_3$ systems has also been observed by K.R.S. Preethi Meher et al. and V. Trepakov et al. [34, 35]. According to the literature data, the position of the mentioned peak at ~750 cm^{-1} does not correspond to the position of any of the stronger modes of manganese oxide (MnO, MnO_2 or Mn_3O_4) and does not correspond to pure $SrTiO_3$ [36, 37]. This peak is not present in the spectrum of Mn_3O_4 and is barely noticeable in the spectra of some crystalline modifications of MnO_2. Since the peak at ~750 cm^{-1} is clearly visible in the spectra of doped samples, where its intensity increases with increasing dopant concentration and this is not accompanied with the occurrence or increased intensity of any of the two strongest MnO_2 modes, it may be concluded that the observed change in the intensity of this peak with the increasing value of x indicates the incorporation of Mn ions into the $SrTiO_3$ lattice.

As it can be seen from Fig. 9, the application of mechanical activation leads to a more pronounced increase in the intensity of the peak at ~750 cm^{-1}, indicating that the activation causes an effectively higher incorporation of the dopant into the strontium-titanate lattice.

IV. Conclusion

In summary, this paper offers an important overview of the role and the advantages of nonresonant Raman spectroscopy, which is presented using the examples that illustrate the analyses of structural changes in electronic materials obtained from mechanically activated $BaTiO_3$ and $SrTiO_3$ powders. The doping effect, the obtaining of nanocomposites with an enhanced share of the electroactive crystalline phase of a polymer matrix and the obtaining of hexaferrite as a multiferroic material are considered in the paper, as well. The influence of the laser beam power on the spectra is also discussed.

Acknowledgment

This work was supported by the Ministry of Education, Science and Technological Development of the Republic of Serbia under the contracts 451-03-68/2020-14/200105 and NSF-RISE 1829245, NSF-PREM 1523617, and NSF CREST 1345219 awards.

References

[1] D. J. Gardiner, P. R. Graves (Editors); with contributions by H. J. Bowley [and five others], *Practical Raman Spectroscopy*, Berlin, Germany: Springer-Verlag, 1989.

[2] B. Schrader, *Infrared and Raman Spectroscopy - Methods and Applications*, Weinheim, Germany: VCH, 1995

[3] R. Merlin, A. Pinczuk, W. H. Weber, *Overview of Phonon Raman Scattering in Solids*, Chapter in *Raman Scattering in Materials Science*, Springer Series in Materials Science, book series vol. 42, pp. 1-29, Springer, Berlin, Heidelberg, Germany: Springer, 2000.

[4] B. Ertuğ, "The overview of the electrical properties of barium titanate", *Am. J. Eng. Res.*, vol. 2, no. 8, pp. 01-07, 2013.

[5] E Guo, L Yin, "Tailored $SrTiO_3/TiO_2$ heterostructures for dye-sensitized solar cells with enhanced photoelectric conversion performance", *J. Mater. Chem. A*, vol. 3, no. 25, pp. 13390-13401, May 2015.

[6] J. H. Jeon, Y. D. Hahn, H. D. Kim, "Microstructure and dielectric properties of barium-strontium titanate with a functionally graded structure", *J. Eur. Ceram. Soc*, vol. 21, no. 10-11, pp. 1653-1656, August 2001.

[7] X. Qiu, "Patterned piezo-, pyro- and ferroelectricity of poled polymer electrets", *J. Appl. Phys*., vol. 108, no. 1, pp. 011101, July 2010.

[8] V. Tomer, E. Manias, C.A. Randal, "High field properties and energy storage in nanocomposite dielectrics of poly(vinylidene fluoride-hexafluoropropylene)", *J. Appl. Phys.*, vol. 110, no. 4, pp. 044107, August 2011.

[9] A. Rani, J. Kolte, S. S. Vadla, P. Gopalan, "Structural, Electrical, Magnetic and Magnetoelectric properties of Fe doped $BaTiO_3$ ceramics", *Ceram. Int*., vol. 42, no. 7, pp. 8010-8016, May 2016.

[10] F. M. Silva Junior, C. W. A. Paschoal, "Spin-phonon coupling in $BaFe_{12}O_{19}$ M-type hexaferrite", *J. Appl. Phys*., vol. 116, no. 24, pp. 244110, December 2014.

[11] G. Tan, X. Chen, "Structure and multiferroic properties of barium hexaferrite ceramics", *Journal of Magnetism and Magnetic Materials*, vol. 327, pp. 87-90, February 2013.

[12] J. Li, H. Zhang, Y. Liu, Q. Li, H. Zhou, H. Yang, "Phase formation, magnetic properties and Raman spectra of Co-Ti co-substitution M-type barium ferrites", *Appl. Phys. A*, vol. 119, no. 2, pp. 525-532, January 2015.

[13] D. Choudhury, S. Mukherjee, P. Mandal, A. Sundaresan, U. V. Waghmare, S. Bhattacharjee, R. Mathieu, P. Lazor, O. Eriksson, B. Sanyal, P. Nordblad, A. Sharma, S. V. Bhat, O. Karis, D. D. Sarma, "Tuning of dielectric properties and magnetism of $SrTiO_3$ by site-specific doping of Mn", *Phys. Rev. B*, vol. 84, no. 12-15, pp. 125124, September 2011.

[14] T. Yan, Z. G. Shen, W. W. Zhang, J. F. Chen, "Size dependence on the ferroelectric transition of nanosized $BaTiO_3$ particles", *Mater. Chem. Phys*., vol. 98, no. 2-3, pp. 450-455, August 2006.

[15] Y. I. Kim, J. K. Jung, and K. S. Ryu, "Structural Study of Nano $BaTiO_3$ Powder by Rietveld Refinement", *Mater. Res. Bull*., vol. 39, no. 7-8, pp. 1045-1053, June 2004.

[16] W. Peukert, "Material properties in fine grinding", *Int. J. Miner. Process*, vol. 74, Supplement, pp. S3-S17, December 2004.

[17] V. P. Pavlović, B. Vlahović, D. Kosanović, M. Dukić, M. Wu, V. B. Pavlović, "Mechanically Activated Ferroelectric Materials", Proc. of 3rd International conference on Electrical, Electronic and Computing Engineering – IcETRAN 2016, Zlatibor, Serbia, pp. NMI1.1.1-8, June 13-16, 2016.

[18] T. Hoshina, H. Kakemoto, T. Tsurumi, S. Wada, "Size and Temperature Induced Phase Transition Behaviors of Barium Titanate Nanoparticles", *J. Appl. Phys.*, vol. 99, no. 5, pp. 054311, March 2006.

[19] R. Naik, J. J. Nazarko, C. S. Flattery, U. D. Venkateswaran, V. M. Naik, M. S. Mohammed, G. W. Auner, J. V. Mantese, N. W. Schubring, A. L. Micheli, and A. B. Catalan, "Temperature Dependence of the Raman Spectra of Polycrystalline $Ba_{1-x}Sr_xTiO_3$", *Phys. Rev. B*, vol. 61, no. 17, pp. 11367-11372, May 2000.

[20] V. P. Pavlovic, M. V. Nikolic, V. B. Pavlovic, J. Blanusa, S. Stevanovic V. V. Mitic, M. Scepanovic, "Raman Responses in Mechanically Activated $BaTiO_3$", *J. Am. Ceram. Soc.*, vol. 97, no. 2, pp. 601-608, January 2014.

[21] B. Wang and L. Zhang, "Size Effects on Structure and Raman Spectra of $BaTiO_3$ Thin Film", *Phys. Status Solidi A*, vol.169, no.1, pp. 57-62, September 1998.

[22] M. Zhang, J. Yu, J. Chu, Q. Chen, and W. Chen, "Microstructures and Photoluminescence of Barium Titanate Nanocrystals Synthesized by the Hydrothermal Process", *J. Mater. Process. Technol*., vol. 137, no. 1-3, pp. 78-81, June 2003.

[23] V. P. Pavlovic, V. B. Pavlovic, B. Vlahovic, D. K. Bozanic, J. D. Pajovic, R. Dojcilovic and V. Djokovic, "Structural properties of composites of polyvinylidene fluoride and mechanically activated $BaTiO_3$ particles", *Physica Scripta*, T157, pp. 014006-1-5, November 2013.

[24] R. Gregorio, "Determination of the α, β and γ crystalline phases of poly(vinylidene fluoride) films prepared at different conditions", *J. Appl. Polym. Sci.*, vol. 100, no. 4, pp. 3272-3279, May 2006.

[25] N. J. Ramer, T. Marrone, K. Stiso, "Structure and vibrational frequency determination for α-poly (vinylidene fluoride) using density-functional theory", *Polymer*, vol. 47, no. 20, pp. 7160-7165, September 2006.

[26] T. Boccaccio, A. Bottino, G. Capannelli, P. Piaggio, "Characterization of PVDF membranes by vibrational spectroscopy", *J. Membr. Sci*., vol. 210, no. 2, pp. 315-329, December 2002.

[27] V. P. Pavlović, D. Popović, J. Krstić, J. Dojčilović, B. Babić, V. B. Pavlović, "Influence of Mechanical Activation on the Structure of Ultrafine $BaTiO_3$ Powders", *J. Alloys Compd*., vol. 486, no. 1-2, pp. 633-639, July 2009.

[28] D. Kosanović, N. Obradović, V. P. Pavlović, S. Marković, A. Maričić, G. Rasić, B. Vlahović, V. B. Pavlović, M. M. Ristić, "The influence of mechanical activation on the morphological changes of $Fe/BaTiO_3$ powder", *Materials Science and Engineering B: Advanced Functional Solid-State Materials*, vol. 212, pp. 89-95, October 2016.

[29] D. L. A. de Faria, S. Venaüncio Silva, M. T. de Oliveira, "Raman microspectroscopy of some iron oxides and oxyhydroxides", *Journal of Raman Spectroscopy*, vol. 28, no. 11, pp. 873-878, November 1997.

[30] D. Kosanović, V. A. Blagojević, A. Maričić, S. Aleksić, V. P. Pavlović, V.B. Pavlović, B. Vlahović, "Influence of mechanical activation on functional properties of barium hexaferrite ceramics", *Ceramics International*, vol. 44, no. 6, pp. 6666-6672, April 2018.

[31] D. A. Vinnik, V. E. Zhivulin, A. Yu. Starikov, S. A. Gudkova, E. A. Trofimov, A. V. Trukhanov, S. V. Trukhanov, V. A. Turchenko, V. V. Matveev, E. Lahderanta, E. Fadeev, T. I. Zubar, M. V. Zdorovets, A. L. Kozlovsky, "Influence of titanium substitution on structure, magnetic and electric properties of barium hexaferrites $BaFe_{12-x}Ti_xO_{19}$", *Journal of Magnetism and Magnetic Materials*, vol. 498, pp. 166117, March 2020.

[32] J. Živojinović, V. P. Pavlović, D. Kosanović, S. Marković, J. Krstić, V. A. Blagojević, V. B. Pavlović, "The Influence of Mechanical Activation on Structural Evolution of Nanocrystalline $SrTiO_3$ Powders", *Journal of Alloys and Compounds*, vol. 695, pp. 863-870, February 2017.

[33] Y. L. Du, G. Chen, M.S. Zhang, "Investigation of structural phase transition in polycrystalline $SrTiO_3$ thin films by Raman spectroscopy", *Solid State Communications*, vol. 130, no. 9, pp. 577-580, June 2004.

[34] K. R. S. Preethi Meher, C. Bogicevic, P. E. Janolin, K. B. R. Varma, "Synthesis dependent characteristics of $Sr_{1-x}Mn_xTiO_3$ (x=0.03, 0.05, 0.07 and 0.09) ", *J. Solid State Chem.*, vol. 192, pp. 296-304, August 2012.

[35] V. Trepakov, M. Makarova, O. Stupakov, E. A. Tereshina, J. Drahokoupil, M. Cernanský, Z. Potucek, F. Borodavka, V. Valvoda, A. Lynnyk, A. Jäger, L. Jastrabik, A. Dejneka, "Synthesis, structure and properties of heavily Mn-doped perovskite-type $SrTiO_3$ nanoparticles", Materials Chemistry and Physics, vol. 143, no. 2, pp. 570-577, January 2014.

[36] P. Y. Kuang, M. H. Liang, W. Y. Kong, Z. Q. Liu, Y. P. Guo, H. J. Wang, N. Li, Y. Z. Su, S. Chen, "Anion-assister one-pot synthesis of 1D magnetic α- and β-MnO_2 nanostructures for recyclable water treatment application", *New J. Chem.*, vol. 39, no. 4, pp. 2497-2505, January 2015.

[37] B. J. Rani, M. Ravina, G. Ravi, S. Ravichandran, V. Ganesh, R. Yuvakkuma, "Synthesis and characterization of Hausmannite (Mn_3O_4) nanostructures", *Surfaces and Interfaces*, vol. 11, pp. 28-36, June 2018.

Structural and Magnetic Features of a FeCo-2V Alloy Processed by Metal Injection Molding

Borivoje Nedeljković, Nebojša Mitrović, *member IEEE*, Vladimir Pavlović

***Abstract*— In this paper the characterization of FeCo-2V alloys processed by metal injection molding (MIM) technology was investigated. The feedstock for MIM was prepared by mixing FeCoV powder with a low viscosity binder. Sintering of brown samples was performed during 3.5 hours from 1370 ^{O}C to 1460 ^{O}C in hydrogen atmosphere in order to attain the appropriate functional properties.**

Microstructure and magnetic hysteresis B(H) of toroidal samples were investigated as a function of sintering temperature. An optimum magnetic properties were observed after sintering at temperature of 1370 ^{O}C. Magnetic properties were analyzed as frequency dependent in operating frequency range from 5 Hz to 60 Hz.

Index Terms — Metal injection moulding technology; FeCoV alloy, Structural properties, Magnetic properties

I. Introduction

TECHNOLOGY of powder injection moulding (PIM) can offer very efficient manufacturing of ceramic or metallic parts with complex geometric shapes. Alloys that contain metal elements were produced by variation of PIM technology named metal injection molding (MIM) [1-3]. MIM as well as direct laser metal sintering (DLMS) process (where mixed metal powders are consolidated by laser in a single production step [4, 5]) are common and useful technologies for commercial production of many magnetic elements. Plenty of combinations of powders mixture, binders, molding techniques, debinding and sintering parameters, make MIM technology suitable for magnetic materials industry as it enables easier production of complex cores compared to the classical routes [6-8]. Unique magnetic properties can be obtained by mechanochemical processing of nanostructured $Fe_{49}Co_{49}V_2$ alloy [9, 10] as well as composite preparation [11].

Silva et. all [8] investigated equiatomic Fe50Co50 alloy produced by MIM without V addition and concluded that the elimination of vanadium can improve magnetic properties. It is possible to substantial decrease sintering temperature (980 ^{O}C instead of common sintering temperature of 1330 ^{O}C). Microstructure of the V containing alloy exhibits smaller grain size with increased porosity as a main obstacles for magnetic domains movement resulting in the magnetic hardening. However, binary FeCo alloys are very brittle [12], and addition up to 2 % wt. of vanadium improves strength and ductility. Commercial functional material must poses both good mechanical and magnetic properties.

Advanced soft magnetic materials should exhibit a high saturation magnetic induction B_S and relative magnetic permeability μ_r as well as low core losses P_{core} and coercive force H_C. High Curie temperature T_C, corrosion resistance and good mechanical properties are also very very important for some applications. Devices prepared from FeCo-2V alloy are usually exploited under extreme conditions (high operating temperature with high stress) and their functionality is associated with the unique combination of magnetic and mechanical properties. Iron-cobalt based alloys exhibit unique combination of high B_S and T_C as well as high corrosion resistance [12, 13]. The semi-hard magnetic alloy FeCo-2V is widely used in automation and electronics many of these parts are with complex shapes. Therefore, FeCoV alloy ferromagnetic parts for high temperature applications can be cost-effectively produced by MIM route.

II. Experimental

In these experiments the feedstock was prepared by mixing the starting very fine powder and binder system that is easily removable by solvent and thermal debinding.

The investigated toroidal samples were produced by a Battenfeld HM 600/130 hydraulic drive injection moulding machine. A green cylindrical component with a central hole has 10 mm internal diameter, 18 mm external diameter and 28 mm length.

The injected green samples were first subjected to solvent debinding and subsequent thermal debinding followed by sintering with a holding time of 3.5 hours. The applied sintering procedure and atmosphere were taken from the classical procedure with pressed samples with a small modification of the initial stage of sintering to include thermal debinding. Secondary thermal debinding at optimized temperatures (up to 800 ^{O}C) and sintering in the temperature range 1370 ^{O}C - 1460 ^{O}C were performed on brown samples in a hydrogen atmosphere.

After this initial preparation the obtained samples had internal diameter of 8.5 mm and external diameter of 16 mm. Samples about 7.5 mm high were cut from the center section of the sintered piece, in order to achieve better measurement accuracy. Magnetic properties on toroidal core samples were measured at room temperature by Brockhaus Tester MPG 100 D that is common used for examination of

Borivoje Nedeljković – University of Kragujevac, Faculty of Technical Sciences in Čačak, Svetog Save 65, Serbia (e-mail: borivoje.nedeljkovic@ ftn.kg.ac.rs)

Nebojša Mitrović – University of Kragujevac, Faculty of Technical Sciences in Čačak, Svetog Save 65, Serbia (e-mail: nebojsa.mitrovic@ ftn.kg.ac.rs).

Vladimir Pavlović – Institute of Technical Sciences of SASA, Knez Mihailova 35/IV, Belgrade, (e-mail: vladimir.pavlovic@ itn.sanu.ac.rs).

soft magnetic materials. The main properties such as coercive force H_C, saturation induction B_S and remanent induction B_r were determined from B-H loops. Maximum excitation was H_{max}=6 kA/m at driving frequency set from 5 Hz to 60 Hz.

X-ray diffractograms of the samples after sintering were obtained using a Philips PW 1050 with $Cu_{K\alpha}$ radiation (λ=0.154 nm) and a step/time scan mode of 0.05 ^{O}/1 s. Scanning electron microscopy (SEM) JEOL JSM-6390 LV was used for microstructural characterization of the investigated samples after sintering process.

III. Results and Discussion

XRD diffraction patterns of FeCo-2V alloy samples sintered from 1370 ^{O}C to 1460 ^{O}C in hydrogen atmosphere are presented in Fig. 1. The clear evidence of the α-FeCo crystalline phase by main diffraction peak around 2θ = 45 ^{O} is found for all investigated samples. An increase of sintering temperature is also folowed by more intensive diffraction peaks that is especially evidenced on patterns 1.c and 1.d for samples sintered at 1430 ^{O}C and 1460 ^{O}C, respectively.

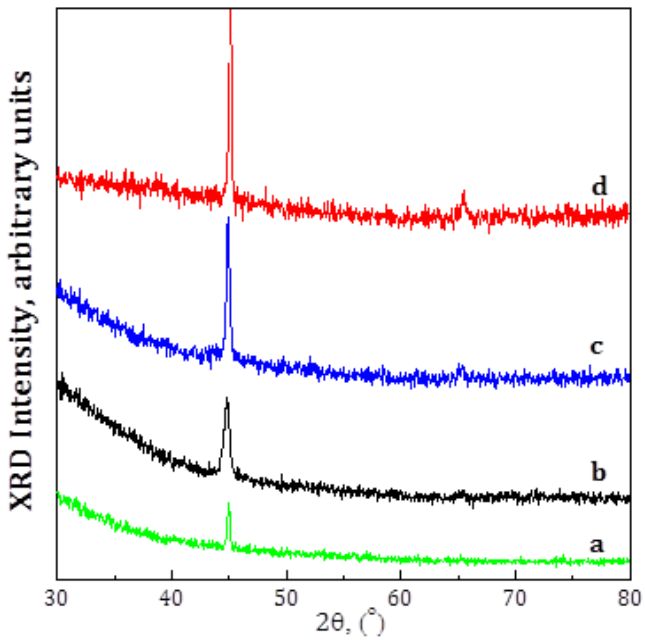

Fig.1. XRD diffractograms of FeCo-2V alloy samples sintered with a holding time of 3.5 hours at temperature a) 1370 ^{O}C b) 1400 ^{O}C, c) 1430 ^{O}C and d) 1460 ^{O}C in hydrogen atmosphere.

Fig. 2. presents the iron α-Fe (A2), cobalt ε-Co (A3) and α'-FeCo (B2) crystal phases, with appropriate magnetic features [14]. Evolved α'-FeCo (B2) crystal phase is characterized by extremely high Curie temperature (T_c = 1390 K that is even a little bit higher than the pure cobalt). Therefore, FeCo alloys with this crystal phase poses unique property of feromagnetic behavior at high exploiting temepeartures. Further, it can be observed increase in magnetic moment for both atoms (α-Fe iron μ_{Fe} =2.218 μ_B/atom → α'-FeCo μ_{Fe} =3.0 μ_B/atom, ε-Co cobalt μ_{Co} =1.716 μ_B/atom → α'-FeCo μ_{Co} =1.8 μ_B/atom), which results in very high value of magnetic induction saturation B_S over 2 T.

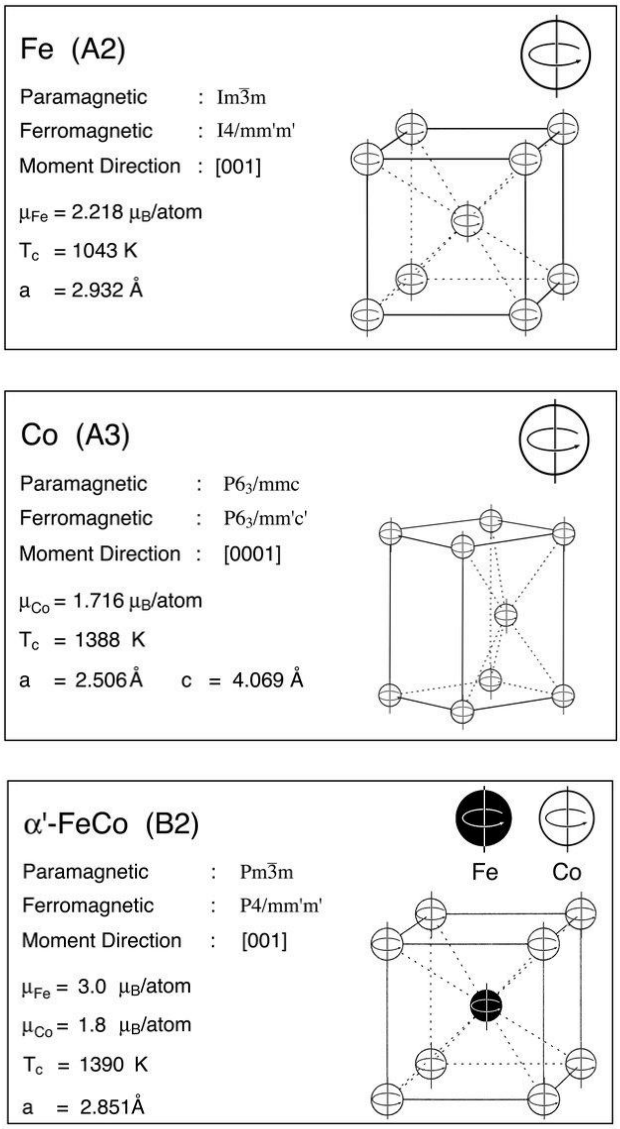

Fig.2. Crystal structures for iron α-Fe (A2), cobalt ε-Co (A3) and α'-FeCo (B2) phases, with magnetic features [14].

The SEM micrographs obtained from the surface of the investigated sintered samples are shown in Fig. 3. It can be seen that the powder particles were melted proportionaly to the sintering temperature in the range from 1370 ^{O}C to 1460 ^{O}C (Figs. 3.a, 3.b, 3.c and 3.d).

The picture of the sample sintered at the highest temperature 1460 ^{O}C unequivocally shows that the particles were completely melted. This is in good correlation with XRD pattern in Fig 1.d which exhibits the most intensive crystallization.

Fig. 4. shows the B(H) hysteresis loops broadening for minor curves (H_{max} = 6 kA/m) for FeCo-2V sample sintered at 1370 ^{O}C obtained at frequencies of 5 Hz, 10 Hz, 20 Hz, 40 Hz, 50 Hz and 60 Hz. It is well known that an increase in frequency leads to an increase in core power losses P_{tot} due to hysteresis losses P_h, normal eddy current losses as well as anomalous eddy current losses, respectively: $P_{tot} = P_h + P_e + P_{an}$.

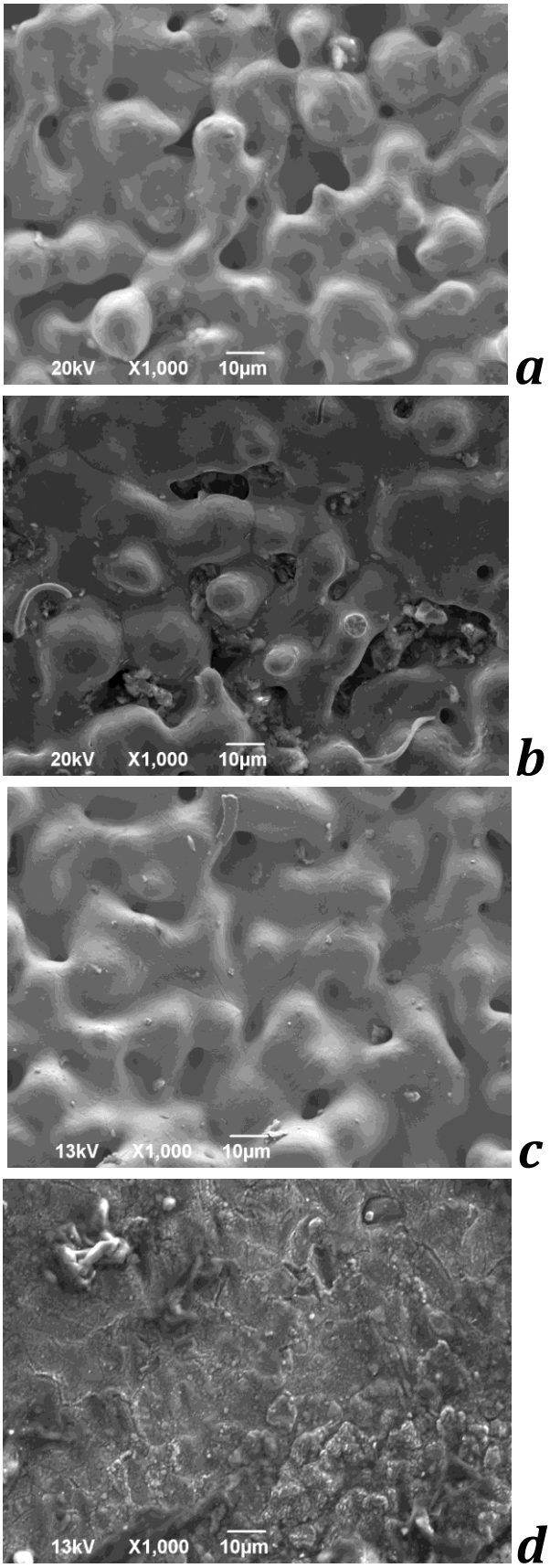

Fig. 3. Microstructures of FeCo-2V alloy samples sintered with a holding time of 3.5 hours at temperature a) 1370 ^{O}C b) 1400 ^{O}C, c) 1430 ^{O}C and d) 1460 ^{O}C in hydrogen atmosphere.

Fig. 5. shows the B(H) hysteresis loops broadening for FeCo-2V sample sintered at 1400 ^{O}C obtained at frequencies of 5 Hz, 10 Hz, 20 Hz, 40 Hz, 50 Hz (H_{max} = 6 kA/m), as well as anomalous shape of dynamic loop at 60 Hz.

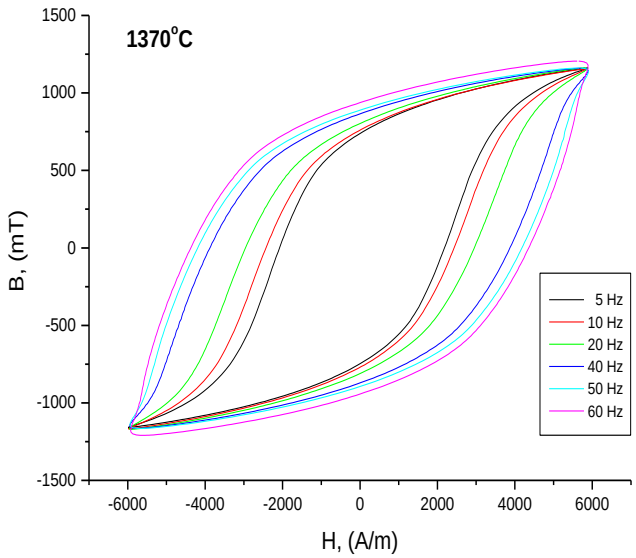

Fig. 4. The B(H) hysteresis loops broadening for FeCo-2V sample sintered at 1370 ^{O}C obtained at frequencies of 5 Hz, 10 Hz, 20 Hz, 40 Hz, 50 Hz and 60 Hz (H_{max} = 6 kA/m).

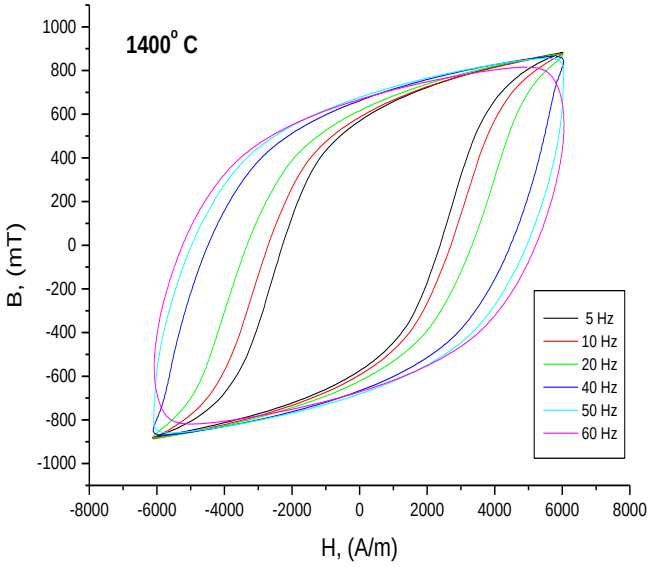

Fig. 5. The B(H) hysteresis loops broadening for FeCo-2V sample sintered at 1400 ^{O}C obtained at frequencies of 5 Hz, 10 Hz, 20 Hz, 40 Hz, 50 Hz and 60 Hz (H_{max} = 6 kA/m).

It is performed numerical analysis of corecitive force on frequency $H_C(f)$, with the model already proposed by Grössinger et al [15]:

$$H_C(f) = a + b \cdot f^{1/2} + c \cdot f \qquad (1)$$

where coefficient ***a*** correspond to the zero frequency coercivity that is extrapolated from the low frequency numerical data. The next two coefficients ***b*** and ***c*** describes the normal eddy currents and anomalous eddy currents, respectively.

The results of numerical analysis of corecitive force on frequency for samples sintered at 1370 ^{O}C and 1400 ^{O}C are presented on Fig. 6. (numerical data from the hysteresis lops obtained at frequencies of 5 Hz, 10 Hz, 20 Hz, 40 Hz, 50 Hz and 60 Hz (H_m = 6 kA/m) presented on Fig. 4 and Fig. 5).

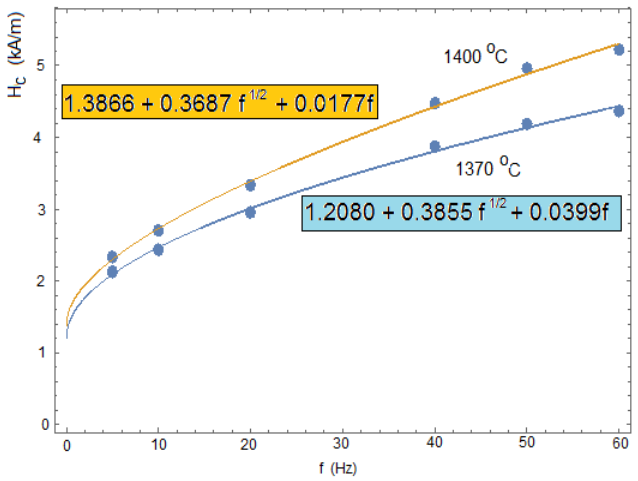

Fig.6. Dependence of coercivity on frequency H_C (f), for FeCo-2V samples sintered at 1370 °C and 1400 °C.

Table I shows the analysis of the anomalous eddy currents at the frequencies of 5 Hz and 50 Hz for samples sintered at 1370 °C and 1400 °C. One can see for sample sintered at 1370 °C at low frequency of 5 Hz anomalous eddy currents influence $H_{Can}(f) = c \cdot f$ is only about 1 % and at high frequency of 50 Hz that influence is about 5 %. For sample sintered at 1400 °C at low frequency of 5 Hz anomalous eddy currents influence is 3.9 %, and at high frequency of 50 Hz that influence is high, i.e. about 18 %. Remanences for both hysteresis loops are similar: 0.77 for 1370 °C and 0.79 for 1400 °C.

Table I.

Zero frequency coercivity H_{CO}, total coercivity H_C, remanence ratio B_r/B_s and anomalous eddy currents influence at the frequencies of 5 Hz and 50 Hz for samples sintered at 1370 °C and 1400 °C.

	$a \cong H_{CO}$ (kA/m)	H_C (kA/m)	B_r/B_s	H_{Can} (f) / H_C (f)
1370 °C	1,208	2,091 (5 Hz)	0.767	1 % (5 Hz)
1400 °C	1,387	2,299 (5 Hz)	0.792	3.9 % (5 Hz)
1370 °C	1,208	4,133 (50 Hz)	0.767	5 % (50 Hz)
1400 °C	1,387	4,880 (50 Hz)	0.792	18 % (50 Hz)

IV. Conclusion

Characterization of near-equiatomic FeCo-based alloy with addition of 2 wt. % vanadium produced by MIM technology was performed. Only α-FeCo crystalline phase is found for all investigated FeCo-2V alloy samples sintered from 1370 °C to 1460 °C in hydrogen atmosphere with a holding time of 3.5 hours. Powder particles sintered at the highest temperature 1460 °C were completely melted.

Magnetic measurements were performed in the operating frequency range from 5 Hz to 60 Hz with observed optimum magnetic properties for sample sintered at 1370 °C.

At high frequency of 50 Hz it is observed anomalous eddy currents influence of only about 5 % (sample sintered at 1370 °C), but for sample sintered at 1400 °C that influence is very high, about 18 %.

Acknowledgment

This study was supported by the Ministry of Education, Science and Technological Development of the Republic of Serbia, and these results are parts of the Grant No. 451-03-68/2020-14/200132 with University of Kragujevac - Faculty of Technical Sciences Čačak.

References

[1] H. Ye, X. Y. Liu, H. Hong, "Fabrication of metal matrix composites by metal injection molding-A review", *Journal of Materials Processing Technology*, 200 (2008) 12–24.

[2] P. Setasuwon, A. Bunchavimonchet, S. Danchaivijit, "The effects of binder components in wax/oil systems for metal injection molding", *Journal of Materials Processing Technology*, 196 (2008) 94–100.

[3] H. Shokrollahi, K. Janghorban, "Soft magnetic composite materials (SMCs)", *Journal of Materials Processing Technology*, 189 (2007) 1–12.

[4] A. Simchi, "Direct laser sintering of metal powders: Mechanism, kinetics and microstructural features", *Materials Science and Engineering: A*, 428 (2006) 148–158.

[5] Z. Ebersold, N. Mitrović, S. Đukić, B. Jordović, A. Peulić, "Defectoscopy of direct laser sintered metals by low transmission ultrasonic frequencies", *Science of Sintering*, 44 (2012) 177-185.

[6] A. Silva, J. A. Lozano, R. Machado, J. A. Escobar, P. A. P. Wendhausen, "Study of soft magnetic iron cobalt based alloys processed by powder injection molding", *Journal of Magnetism and Magnetic Materials*, 320 (2008) e393–e396.

[7] B. Zlatkov, N. Mitrović, MV. Nikolić, A. Maričić, H. Danninger, O. Aleksić, E. Halwax, "Properties of MnZn ferrites prepared by powder injection molding technology", *Materials Science and Engineering B–Advanced Functional Solid-state Materials*, 175 (2010) 217-222

[8] A. Silva, J. A. Lozano, R. Machado, J. A. Escobar, P. A. P. Wendhausen, "Study of soft magnetic iron cobalt based alloys processed by powder injection molding", *Journal of Magnetism and Magnetic Materials*, 320 (2008) e393–e396.

[9] A. Behvandi, H. Shokrollahi, B. Chitsazan, M. Ghaffari, "Magnetic and structural studies of mechanically alloyed nano-structured $Fe_{49}Co_{49}V_2$ powders", *Journal of Magnetism and Magnetic Materials*, 322 (2010) 3932–3937.

[10] B. Chitsazan, H. Shokrollahi, A. Behvandi, O. Mirzaee, "Characterization and magnetic coercivity of nanostructured $(Fe50Co50)_{100-X}V_{X=0,2,4}$ powders containing a small amount of Co_3V intermetallic obtained by mechanical alloying", *Powder Technology*, 214 (2011) 105–110.

[11] B. Weidenfeller, M. Anhalt, W. Riehemann, "Variation of magnetic properties of composites filled with soft magnetic FeCoV particles by particle alignment in a magnetic field", *Journal of Magnetism and Magnetic Materials*, 320 (2008) e362–e365.

[12] T. Sourmail, "Near equiatomic FeCo alloys: Constitution, mechanical and magnetic properties", *Progress in Materials Science*, 50 (2005) 816–880.

[13] G. B. Chon, K. Shinoda, S. Suzuki and B. Jeyadevan, "Order-disorder transformation in Fe50Co50 particles synthesized by polyol process", *Materials Transactions*, 51 (2010) 707-711.

[14] D. E. Laughlin, M. A. Willard, and M. E. McHenry, "Magnetic Ordering: Some Structural Aspects", Vol: Phase Transformations and Evolution in Materials, TMS Annual Meeting Conference, January 2000. Nashville, Tennessee.

[15] R. Grössinger, N. Mehboob, D. Suess, R. Sato Turtelli, and M. Kriegisch, "An eddy-current model describing the frequency dependence of the coercivity of polycrystalline galfenol", *IEEE Transactions on Magnetics*, 48, pp. 3076-3079, 2012.

Magnetoimpedansni efekat CoFeSiB amorfne žice

Jelena Orelj, Nebojša Mitrović, Vladimir Pavlović

Apstrakt— *U radu su prikazana ispitivanja magnetoimpedansnog (MI) efekta žice legure CoFeSiB. XRD rendgenogram pokazuje da legura poseduje potpuno amorfnu strukturu. DTA analizom je uočeno da je legura temperaturski stabilna do oko 540 ^{O}C gde je registovan egzotermni pik procesa kristalizacije. Pojava MI-efekta kod ispitivane žice je uočena na frekvencijama od 5 kHz do 7 kHz. U opsegu frekvencija 700 kHz ÷ 900 kHz ÷ 1 MHz (@ $H_{max} \approx 4.63$ kA/m) registrovan je maksimalni MI–odnos od oko 330 % i skoro identičan oblik krive $\Delta Z(H)/Z$. Najveći MI-odnos od oko 334 % je dobijen pri frekvenciji od 950 kHz i maksimalnom spoljašnjem magnetnom polju od 7.72 kA/m.*

Ključne reči—MI efekat, CoFeSiB amorfna žica, XRD, EDS, DTA, MI element, MI senzor

I. Uvod

PORED svojih atraktivnih magnetno mekih svojstava, amorfne i nanokristalne feromagnetne legure poseduju i specifične električne karakteristike. Elementi koji pokazuju promenu električne otpornosti pod dejstvom spoljašnjeg dc magnetnog polja R(H_{dc}) (magnetoresistance MR effect) imaju niske relativne vrednosti ΔR/R: 0,53 % FeCrNbCuSiB @ 0.8 T [1]; 0,1 % FeVCuSiB @ 23 kA/m [2]. Promene impedanse ΔZ/Z u odgovarajućem frekventnom opsegu mogu dostići nekoliko stotina procenata (giant magneto impedance (GMI) effect): 506 % CoFeNiMoBSi @ 8 kA/m [3], 1200 % CoFeBSi @ 15 kA/m [4]. Stoga su MI-elementi veoma pogodni za brojne primene u senzorici: sistemi bezbednosti, elektronski kompasi, navigacije/GPS, senzori rotacije, biomagnetna merenja, ... [5-7].

MI-efekat je otkriven tokom devedesetih godina dvadesetog veka kod amorfnih FeCoSiB žica [8], a kasnije je pažnja istraživača okrenuta i ka planarnoj geometriji [9]; naročito ka nanokristalnim trakama i filmovima načinjenih od legura na bazi gvoždja sistema FINEMET Fe**M**CuSiB, **M** = Nb, Mo, Cr, Ta, Zr, V [10, 11].

Najveće osetljivosti u oblasti niskih vrednosti magnetnih polja poseduju amorfne žice legura na bazi kobalta [12-14], pa je stoga jasna njihova najveća atraktivnost za istraživanje. Dok nanokristalne legure na bazi gvoždja postižu svoje odlične karakteristike tek nakon optimalnih termomagnetnih ili termomehaničkih tretmana (tokom kojih se formira fina nanokristalna struktura u amorfnoj matrici), legure na bazi kobalta imaju izvanredne magnetno-meke performanse sa potpuno amorfnom strukturom. Jedan od nedostataka uzoraka na bazi gvoždja nakon nanokristalizacije je slabljenje mehaničkih svojstava [15, 16], što daje bitnu prednost za primenu amorfnim legurama na bazi kobalta.

Jelena Orelj – Fakultet tehničkih nauka u Čačku, Univerziteta u Kragujevcu, Svetog Save 65, Srbija (e-mail: jelena.orelj@ftn.kg.ac.rs.)

Nebojša Mitrović – Fakultet tehničkih nauka u Čačku, Univerziteta u Kragujevcu, Svetog Save 65, Srbija (e-mail: nebojsa.mitrovic@ftn.kg.ac.rs).

Vladimir Pavlović – Institut tehničkih nauka SANU, Beograd, Knez Mihailova 35, Srbija (e-mail: vladimir.pavlovic@itn.sanu.ac.rs).

Promena MI je povezana sa pojavom skin efekta kod feromagnetnih materijala. Naime, na dubini prodiranja δ_m

$$\delta_m = \sqrt{\frac{\rho}{\pi \cdot \mu \cdot f}} \qquad (1)$$

kod magnetno mekih materijala sa niskim vrednostima specifične električne otpornosi $\boldsymbol{\rho}$, visokim vrednostima magnetne permeabilnosti $\boldsymbol{\mu}$ a pri relativno visokim frekvencijama $\boldsymbol{f}$, amplituda vektora gustine struje opadne na **1/e** svoje vrednosti uz površinu uzorka [17]. Usled vihornih struja tok naelektrisanja je potisnut ka površini uzorka (skin efekat) što dovodi do povećanja impredanse. Frekvencija pri kojoj dubina prodiranja postaje manja od poluprečnika žice (δ_m < a) se naziva kritična frekvencija [18, 19], tako da se pri daljem povećanju učestanosti zapažaju fenomeni MI-efekta.

Na slici 1. je prikazana principijelna šema merenja magnetoimpedanse amorfne žice u spoljašnjem dc magnetnom polju generisanom sistemom 1D-Helmholtzovih kalemova.

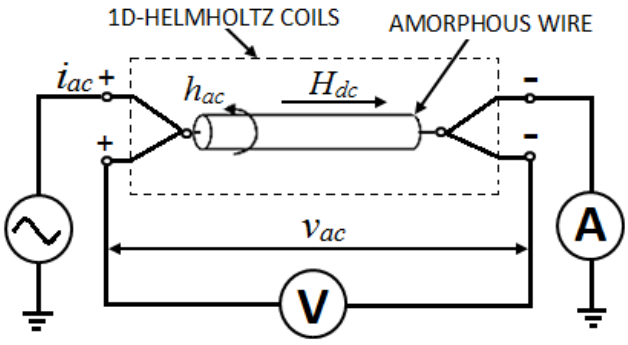

Sl. 1. Šema eksperimenta merenja magnetoipedanse amorfne žice.

Impedansa uzorka amorfne žice je količnik trenutnih vrednosti naizmeničnog napona $\boldsymbol{v}_{ac}$ i naizmenične struje $\boldsymbol{i}_{ac}$, a korišćenjem Maksvelovih jednačina [11, 20] dolazi se do izraza [18]:

$$Z = R + jX = \frac{1}{2} \cdot R_{dc} \cdot (ka) \cdot \frac{J_0(ka)}{J_1(ka)} \qquad (2)$$

gde je $\boldsymbol{R_{dc}}$ električni otpor; R i X realni i imaginarni deo impedanse Z; J_0 i J_1 Beselove funkcije nultog i prvog reda prve vrste, k = (1+j)/δ_m; j^2 = -1.

Spoljašnje longitudinalno dc magnetno polje $\boldsymbol{H_{ex}}$ i cirkularno ac magnetno polje $\boldsymbol{h_{ac}}$ (indukovano protokom naizmenične struje $\boldsymbol{i}_{ac}(t)=I_{cc}\cdot\sin(\omega t)$) utiču na promenu magnetne permabilnosti $\boldsymbol{\mu}$, tako da je impedansa ispitivanog uzorka funkcija tri eksperimentalna parametra Z = Z (f, $\boldsymbol{H_{ex}}$, $\boldsymbol{I_{cc}}$). Intenzitet cirkularnog ac magnetnog polja $\boldsymbol{h_{ac}}$ je:

$$h_{ac}(r,t) = \frac{I_{cc} \cdot r}{2 \cdot \pi \cdot a^2} \cdot \sin \varpi t \qquad (3)$$

gde je $\boldsymbol{r}$ radijalna koordinata, $0 < \boldsymbol{r} \leq a$.

Uticaj spoljašnjeg magnetnog polja $\boldsymbol{H_{ex}}$ na dubinu prodiranja δ_m i relativnu magnetnu permeabilnost $\boldsymbol{\mu_r}$ je prikazan na slici 2. [7]. S obzirom da magnetna permeabilnost (pri konstantnoj frekvenciji $\boldsymbol{f}$ i pri konstantnoj amplitudi struje napajanja $\boldsymbol{I_{cc}}$) opada sa porastom magnetnog polja, dolazi do povećanja dubine prodiranja, što konačno uzrokuje smanjenje impedanse uzorka žice Z($\boldsymbol{H_{ex}}$).

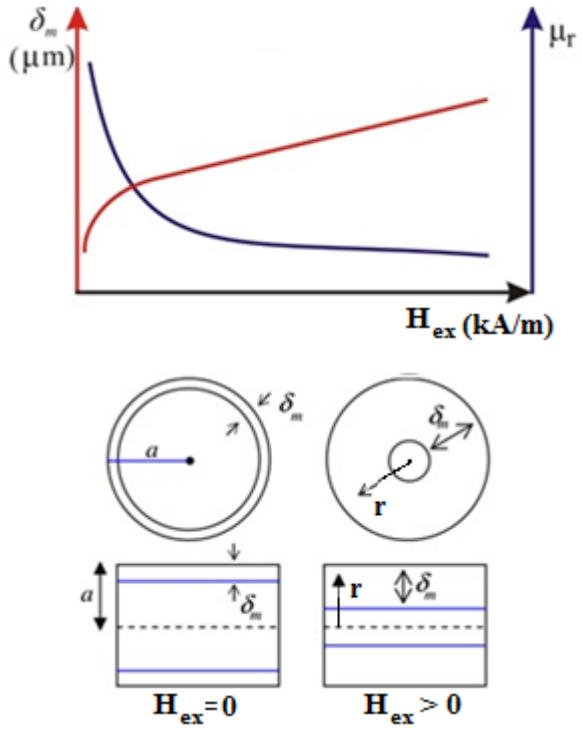

Sl. 2. Promena dubine prodiranja $\boldsymbol{\delta_m}$ i relativne magnetne permeabilnosti $\boldsymbol{\mu_r}$ u zavisnosti od spoljašnjeg dc magnetnog polja $\boldsymbol{H_{ex}}$ kod cilindričnog uzorka magnetno mekog materijala [7].

Na sam MI-efekat direktno utiče interakcija magnetnog polja sa magnetnim domenima čija je struktura posledica unutrašnjih naprezanja nastalih tokom postupka brzog hladjenja rastopa. Putem magnetoelastične interakcije, kod amorfnih žica sa negativnim koeficijentom magnetostrikcije ($\lambda_S < 0$, legure na bazi kobalta) domenska struktura se sastoji od unutrašnjih domena, okruženim cirkularnim domenima naizmenično rasporedjenim duž pravca žice (slika 3. „bamboo domain structure“ [21]).

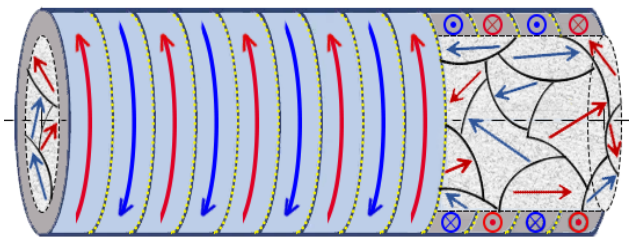

Sl.3. Model domenske strukture kod amorfne žice sa negativnim koeficijentom magnetostrikcije (legure na bazi kobalta), konfiguracija bez dejstva spoljašnjeg magnetnog polja.

Magneto–impedansni (MI) odnos se uglavnom definiše kao relativna promena impedanse uzorka sa promenom spoljašnjeg dc magnetnog polja (H):

$$\Delta Z/Z\ (\%) = 100\ \% \times [Z(H) - Z(H_{max})]/\ Z(H_{max}) \quad (4)$$

gde je Z(H_{max}) impedansa pri maksimalnom magnetnom polju. Uzorak se najčešće pozicionira longitudalno (u pravcu magnetnog polja), tj. u centru sistema 1D-Helmholtzovih kalemova gde je postignuta skoro potpuna homogenost magnetnog polja.

U ovom radu su prikazana istraživanja strukture i MI-efekta legure CoFeSiB u obliku žice, s ciljem procene atraktivnosti njene primene u senzorici.

II. Eksperimentalni deo

Predmet eksperimentalnih ispitivanja je legura CoFeSiB u obliku žice prečnika od oko 100 μm, dobijena metodom brzog hlađenja rastopa u rotirajućem sloju vode na unutrašnjoj površini rotirajućeg diska (in rotating water melt-spinning [7]).

DTA analiza CoFeSiB legure realizovana je na instrumentu „TA SDT 2960“. Rendgenostrukturna XRD istraživanja uzoraka žica vršena su instrumentom Philips PW-1050 sa $Cu_{K\alpha}$ zračenjem (λ = 0,154 nm, step/time scan mode 0.05 ^{O}/s). Ispitivanje mikrostrukture je sprovedeno na skenirajućem elektronskom mikroskopu SEM JEOL JSM-6390 LV opremljenim sa energijski disperzivnim spektrometrom za EDS analizu (Oxford Instruments X-MaxN).

Merenje magnetoimpedanse je izvedeno u homogenom magnetom polju generisanom pomoću 1D-Helmholtzovih kalemova koji daju polje jačine do oko 23 kA/m. Impedansa ispitivanih uzoraka žica dužine 17 mm, merena je po metodi četiri tačke pomoću instrumenta LCR Hi-TESTER HIOKI 3532-50, u frekventnom opsegu od 42 Hz do 1 MHz. Tokom merenja je amplituda struje $\boldsymbol{I_{cc}}$ održavana konstantnom i iznosila je 7 mA. Uzorak amorfne legure CoFeSiB poseduje specifičnu električnu otpornost od ρ = 133 μΩcm.

Na slici 4. je prikazana eksperimentalna postavka merenja magnetoimpedanse uzoraka žica u sistemu 1D-Helmholtzovih kalemova.

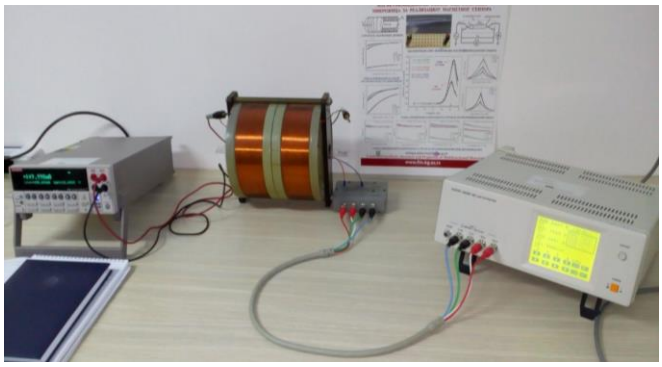

Sl. 4. Eksperimentalna postavka merenja magnetoimpedanse po metodi četiri tačke pomoću instrumenta LCR Hi-TESTER HIOKI 3532-50, f ∈ [42 Hz, 5 MHz].

III. Rezultati i diskusija

Pri ispitivanju amorfnih legura najpre se sprovodi provera njihove strukture (tj. provera amorfnosti XRD difraktogramima) i termičke stabilnosti legure (DTA/DSC analize).

Na slici 5. je prikazan rendgenogram uzorka legure CoFeSiB u obliku žice prečnika 100 μm.

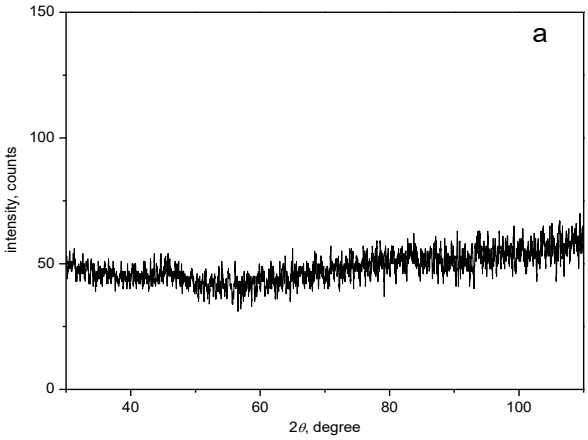

Sl. 5. Rendgenogram uzorka legure CoFeSiB u obliku žice prečnika 100 μm.

Analizom difraktograma X-zračenja uočava se slabo izraženi široki amorfni halo pri uglu $2\theta \approx 45^{O}$, bez naznake pojave kristalnih pikova. Dakle, utvrdjeno je jedino postojanje atomske uredjenosti na blizinu, tj. potvrdjeno je da je ispitivani uzorak legure CoFeSiB potpuno amorfan.

Na slici 6.a su dati rezultati EDS analize, a na slici 6.b je prikazana SEM mikrografija površine uzorka žice.

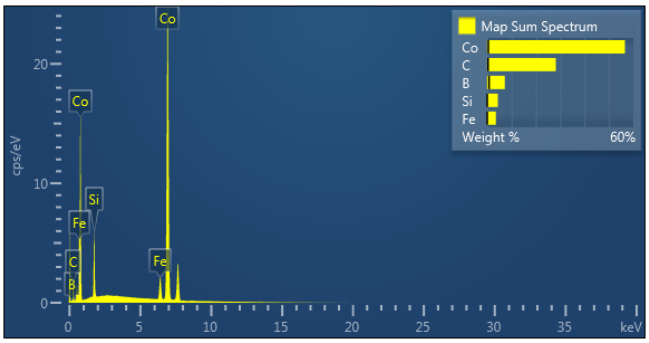

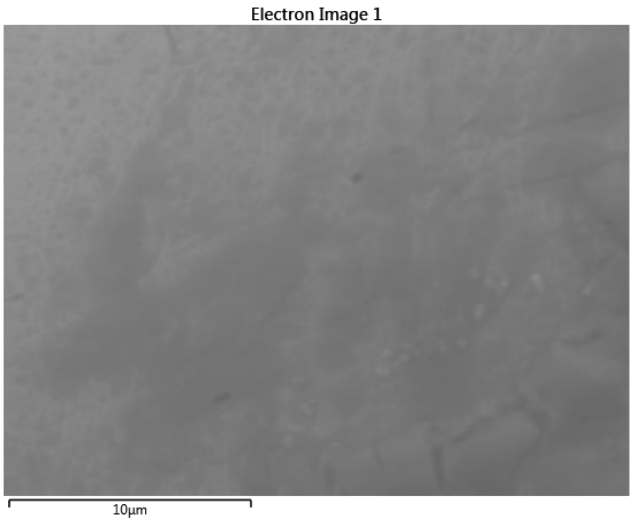

Sl. 6. a) EDS i b) SEM mikrografija površine žice CoFeSiB prečnika 100 μm.

EDS analiza uzorka žice (sl. 6. a) je potvrdila prisutvo svih konstitutivnih elemenata (Co, Fe, Si i B). Na slici 7. su prikazani rezultati mapiranja prisustva pojedinih hemijskih elemenata pomoću EDS detektora.

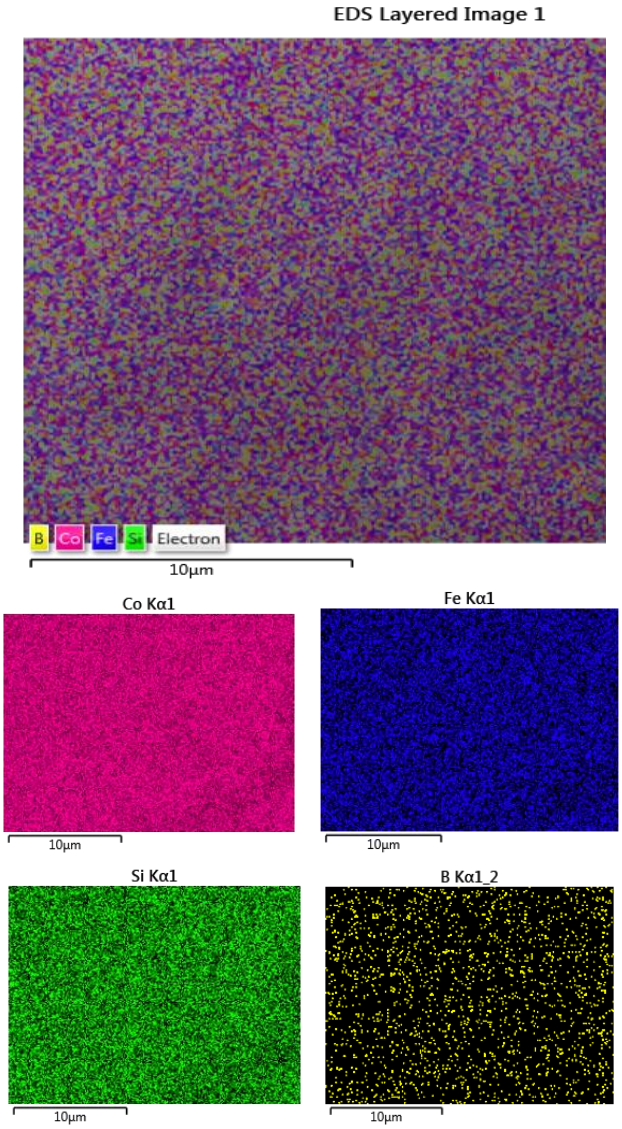

Sl. 7. Mapiranje hemijskih elemenata u leguri pomoću EDS detektora: a) integralna slika svih konstintuenata: b) Co, c) Fe, d) Si i e) B.

Mapiranje prisustva pojedinih konstitutivnih elemenata prikazuje ravnomernu raspodelu atoma svih komponenti legure (sl. 7. a - 7. e).

Na slici 8. je prikazan DTA termogram legure CoFeSiB u obliku žice prečnika oko 100 μm, dobijen pri brzini grejanja od 20 ^{O}C/min.

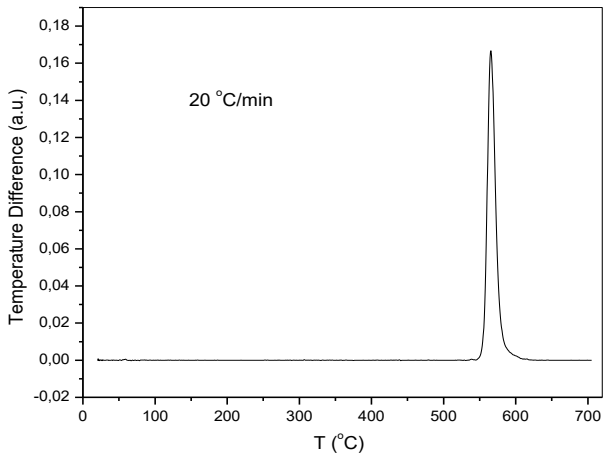

Sl. 8. DTA termogram legure CoFeSiB u obliku žice prečnika oko 100 μm pri brzini grejanja od 20 ^{O}C/min.

Uočeno je da strukturne promene u leguri CoFeSiB počinju na temperaturi oko 540 ^{O}C, što je polazna temperatura egzotermnog kristalizaciona pika prikazanog na slici 8.

Na slici 9. prikazana je zavisnost MI–odnosa od frekvencije pri različitim vrednostima spoljašnjeg dc magnetnog polja $H_{ex} \in$[116 A/m, 7724 A/m]. Kritična frekvencija pri kojoj započinje pojava MI-efekta kod ispitivane žice je 5 kHz ÷ 7 kHz.

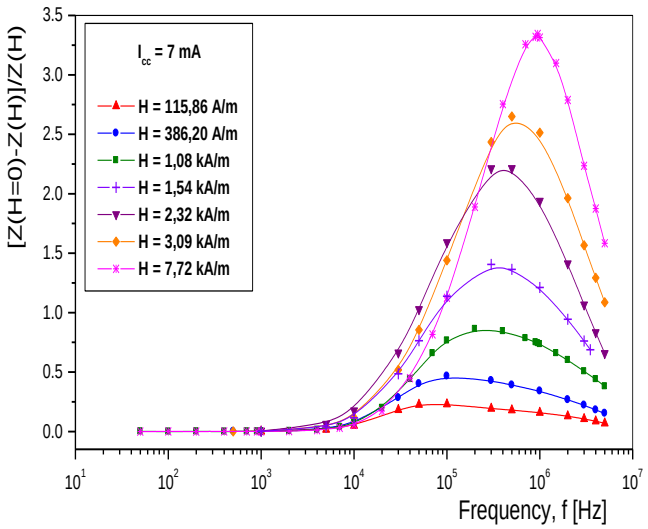

Sl. 9. Frekventna zavisnost MI-odnosa pri različitim vrednostima spoljašnjeg dc magnetnog polja $H_{ex} \in$ [116 A/m, 7724 A/m].

U tabeli I date su maksimalne vrednosti MI-odnosa uz pripadajuće vrednosti maksimalnog spoljašnjeg dc magnetnog polja i odgovarajuće frekvencije.

TABELA I

Maksimalne vrednosti MI – odnosa i pripadajuće frekvencije (pri datoj maksimalnoj vrednosti spoljašnjeg dc magnetnog polja)

H_{ex} (kA/m)	*MI*-odnos (%)	$f_{„max“}$ (kHz)
7.72	334	950
3.09	265	500
2.32	221	500
1.54	140	300
1.08	86	200
0.386	47	100
0.116	23	100

Maksimalni MI-odnos iznosi 334 % pri radnoj frekvenciji od 950 kHz i vrednosti spoljašnjeg dc magnetnog polja H_{max} =7.72 kA/m.

Na slici 10. prikazana je zavisnost MI–odnosa od spoljašnjeg dc magnetnog polja (@ H_{max} = 116 A/m) u frekventnom opsegu f ∈ (20 kHz, 500 kHz). Sve krive pokazuju konstantno smanjenje MI–odnosa usled smanjenja impedanse Z($\boldsymbol{H_{ex}}$) nastale kao posledica povećanja dubine prodiranja $\boldsymbol{\delta_m}$ sa porastom spoljašnjeg dc magnetnog polja $\boldsymbol{H_{ex}}$ (slika 2.). Najveća vrednost MI–odnosa od oko 30 % uočena je pri radnoj frekvenciji od 150 kHz.

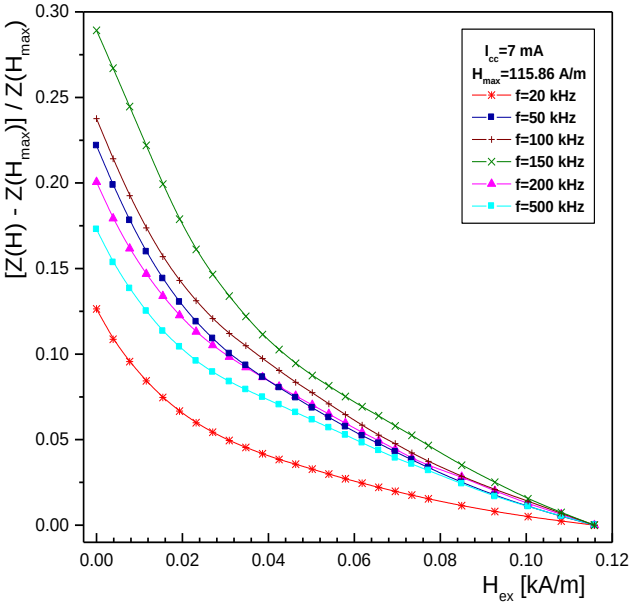

Sl. 10. Zavisnost MI-odnosa od spoljašnjeg dc magnetnog polja pri različitim vrednostima frekvencije f ∈ (20 kHz, 500 kHz) (@ $H_{max} \approx$ 116 A/m).

Na slici 11. je prikazana zavisnost impedanse Z($\boldsymbol{H_{ex}}$) od spoljašnjeg dc magnetnog polja (@ $H_{max} \approx$ 4.63 kA/m) pri različitim vrednostima frekvencije f ∈ (150 kHz, 1 MHz). Primetan je očekivani konstantan porast impedance Z sa povećanjem radne frekvencije.

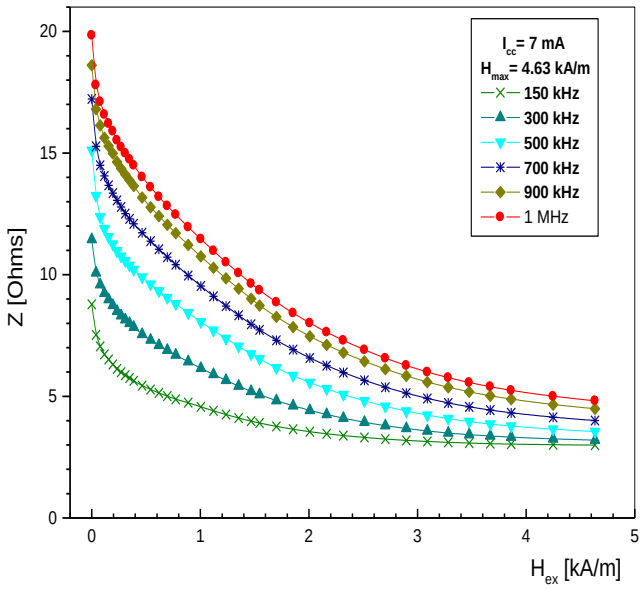

Sl. 11. Zavisnost impedanse Z od spoljašnjeg dc magnetnog polja pri različitim vrednostima frekvencije f ∈ (150 kHz, 1 MHz) (@ $H_{max} \approx$ 4.63 kA/m).

Na slici 12. prikazana je zavisnost MI–odnosa od spoljašnjeg dc magnetnog polja (@ $H_{max} \approx$ 4.63 kA/m) u frekventnom opsegu f ∈ (150 kHz, 1 MHz). Za razliku od promena MI–odnosa pri veoma niskom intenzitetu $\boldsymbol{H_{ex}}$ (slika 10. @ H_{max} = 116 A/m) došlo je do zasićenja porasta MI-odnosa u opsegu radnih frekvencija 700 kHz ÷ 900 kHz ÷ 1 MHz. Za sve tri frekvencije registrovana je slična vrednost maksimalnog MI–odnosa od oko 330 % i skoro identičan oblik krive MI–odnosa.

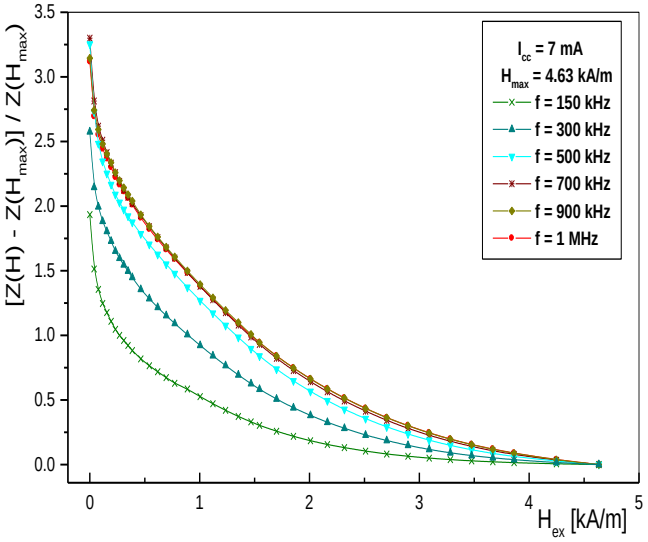

Sl. 12. Zavisnost MI-odnosa od spoljašnjeg dc magnetnog polja pri različitim vrednostima frekvencije f ∈ (150 kHz, 1 MHz) (@ $H_{max} \approx 4.63$ kA/m).

IV. ZAKLJUČAK

Magnetni senzori na bazi magnetoimpedansnog MI-efekta načinjeni od amorfnih / nanokristalnih žica - mikrožica su osnova izuzetnih funkcionalnih karakteristika savremenih električnih naprava. U praksi se koriste i legure na bazi gvoždja i legure na bazi kobalta. Amorfne legure na bazi kobalta u stanju sa optimalnim magnetnim svojstvima poseduju bolja mehanička svojstva u odnosu na nanokristalne legure na bazi gvoždja, te im se posvećuje naročita pažnja. Kod amorfne žice legure CoFeSiB prečnika 100 μm, pojava MI-efekta započinje na oko 5 kHz. Registrovani MI-odnos od čak 344 % pri radnoj frekvenciji od 950 kHz (@ H_{max} =7724 A/m) pokazuje da je ispitivana žica izuzetno atraktivna za primenu u senzorici.

ZAHVALNICA

Ovaj rad je delimično finansiran od strane Ministarstva prosvete, nauke i tehnološkog razvoja Republike Srbije (projekat br. 451-03-68/2020-14/200132 Fakulteta tehničkih nauka u Čačku, Univerziteta u Kragujevcu).

LITERATURA

[1] L. F. Kiss, V. Franco, M. Csontos, L. Peter, C. F. Conde, A. Conde, T. Kemeny, L. K. Varga, I. Bakonyi, "Analysis of the magnetoresistance contributions in a nanocrystallized Cr-doped FINEMET alloy", *Journal of Magnetism and Magnetic Materials*, Vol. 323, pp. 699–707, 2011.

[2] N. Mitrović, "Magnetoresistance of the $Fe_{72}Cu_1V_3Si_{16}B_8$ amorphous alloys annealed by direct current Joule heating", *Journal of Magnetism and Magnetic Materials*, Vol. 262, pp. 302–307, 2003.

[3] P. Gazda, R. Szewczyk, "Influence of Joule-annealing on double-peak GMI effect in Co-based amorphous ribbons", *Acta Physica Polonica* A Vol. 137, pp. 818-820, 2020.

[4] D. Garcıa, V. Raposo, O. Montero, J.I. Iniguez "Influence of magnetostriction constant on magnetoimpedance–frequency dependence", *Sensors and Actuators A*, Vol. 129, pp. 227–230, 2006.

[5] H. Yoshinobu, "Development of amorphous wire type MI sensors for automobile use", *Journal of Magnetism and Magnetic Materials*, Vol. 249, pp. 375–381, 2002

[6] H. Yoshinobu, M. Yamamoto, N. Hamada, A. Shimode, "Magneto-sensitive wire, magneto-impedance element and magneto-impedance sensor", US8610427B2, PATENT, 2013.

[7] M.H. Phan, H.X. Peng, "Giant magnetoimpedance materials: Fundamentals and applications", *Progress in Materials Science*, Vol. 53, pp.323–420, 2008.

[8] L.V. Panina, K. Mohri, "Magneto-impedance effect in amorphous wires", *Applied Physics Letters*, Vol. 65, pp. 1189–1191. 1944.

[9] L. Kraus, "Theory of giant magneto-impedance in the planar conductor with uniaxial magnetic anisotropy", *Journal of Magnetism and Magnetic Materials*, Vol. 195, pp. 764–778, 1999.

[10] M.A.,Willard, M. Daniil, „Nanocrystalline Soft Magnetic Alloys Two Decades of Progress", Handbook of Magnetic Materials, 21, Elsevier, pp. 173-342, 2013.

[11] M. Knobel, M. Vázquez, L. Kraus, "Giant Magnetoimpedance", K.H.J. Buschow, "Handbook of Magnetic Materials", pp. 497- 563, 2003.

[12] J. Liu, H. Shen, D. Xing, and J. Sun, **"**Optimization of GMI properties by AC Joule annealing in melt extracted Co-rich amorphous wires for sensor applications", *Phys. Status Solidi A* Vol. 211, pp. 1577–1582, 2014.

[13] J. Liu, Z. Du, S. Jiang, H. Shen, Z. Li, D. Xing, W. Ma, J. Sun, "Tailoring giant magnetoimpedance effect of Co-based microwires for optimum efficiency by self-designed square-wave pulse current annealing", *Journal of Magnetism and Magnetic Materials* Vol. 385, pp. 145–150, 2015.

[14] L. Gonzalez-Legarreta, P. Corte-Leon, V. Zhukova, M. Ipatov, J.M. Blanco, J. Gonzalez, A. Zhukov, "Optimization of magnetic properties and GMI effect of thin Co-rich microwires for GMI microsensors", Sensors, Vol. 20, 1558, 2020.

[15] A. Lovas, L. Huba, L. Novák, "Pulse heat treatment of FINEMET alloys under tension", *Acta Physica Polonica* A Vol. 126, pp. 100-101, 2014.

[16] K. Csach, J. Miškuf, A. Juríková, V. Ocelík, "Creep of FINEMET ribbons during crystallization", Czechoslovak Journal of Physics Vol. 54, pp. 97-100, 2004

[17] B. Popović, *Elektromagnetika*, Gradjevinska knjiga, Beograd 1980, str. 265.

[18] M. Knobel, M. L. Sanchez, C. Gomez-Polo, P. Marın, M. Vazquez, and A. Hernando, "Giant magnetoimpedance effect in nanostructured magnetic wires", Journal of Applied Physics Vol. 79, pp. 1646–1654, 1996.

[19] N.S Mitrović, S.N. Kane, P.V. Tyagi, S. Roth, „Effect of dc-Joule-heating thermal processing on magnetoimpedance of $Fe_{72}Al_5Ga_2P_{11}C_6B_4$ amorphous alloy", *Journal of Magnetism and Magnetic Materials* Vol. 320, e792-e796, 2008.

[20] L. D. Landau and E. M. Lifshitz, "Electrodynamics of Continuous Media", Pergamon, Oxford, 1975, p. 195

[21] J. Liu, F. Qin, D. Chen, H. Shen, H. Wang, D. Xing, M.H. Phan, J. Sun, ''Combined current-modulation annealing induced enhancement of giant magnetoimpedance effect of Co-rich amorphous microwires'', Journal of Applied Physics Vol. 115, 17A326, 2014.

ABSTRACT

This paper presents the examination of magnetoimpedance MI-effect of CoFeSiB wires. XRD pattern exhibit veak amorphous halo revaling amorphous alloy structure. DTA thermogram shows single exothermic crystallization peak with onset temperature of 540 ^{O}C. The critical frequencies (when δ_m < a) of about 5 kHz ÷ 7 kHz were observed. In the frequency range (700 kHz ÷ 900 kHz ÷ 1 MHz) the similar MI response with maxima of about 330 % is obtained at $H_{max} \approx 4.63$ kA/m. A maximum MI ratio of 334 % is attained at driving frequency of 950 kHz (@ $H_{max} \approx 7.72$ kA/m), revealing investigated CoFeSiB wires perspective as magnetic field sensing elements.

Magnetoimpedance effect of CoFeSiB amorphous wire

Jelena Orelj, Nebojša Mitrović, Vladimir Pavlović

Uticaj sinteze početnih prahova na mikrostrukturna i električna svojstva $BaTiO_3$ keramike

Sandra Veljković, *Student Member, IEEE,* Miloš Đorđević, *Student Member, IEEE,* Vesna Paunović, *Member, IEEE,* Zoran Prijić, *Member, IEEE,* Vojislav Mitić

***Apstrakt* – U ovom radu ispitivana su mikrostrukturna i dielektrična svojstva čistog i La/Mn dopiranog $BaTiO_3$ čiji su početni prahovi dobijeni različitim metodama. Metode dobijanja početnih prahova bile su konvencionalna metoda pripreme polazeći od čistih oksida i Pechini metoda koja polazi od organsko-metalnog kompleksa kao prekursora. Sistemi su sinterovani na 1310°C dva sata. Analiza mikrostrukture nedopirane $BaTiO_3$ keramike pokazala je da je za keramiku dobijenu konvencionalnom metodom karakterističan diskontinualni rast zrna i veličina zrna od 3 do 15 µm, dok je za uzorke dobijene Pechini metodom karakteristična uniformna mikrostruktura i zrna od 1 do 10 µm. Za La/Mn dopiranu keramiku dobijenu Pechini metodom karakteristična je bimodalna mikrostruktura i homogena raspodela aditiva. Dielektrična konstanta ispitivana je u frekventnom opsegu od 100 Hz do 20 kHz. Najveću vrednost i promenu dielektrične konstante sa temperaturom pokazivala je La/Mn dopirana $BaTiO_3$ keramika dobijena Pechini metodom. Dielektrična konstanta ove keramike na Kirijevoj temperaturi bila je 7837. Kiri-Vajsov zakon i modifikovani Kiri-Vajsov zakon korišćeni su za proračun parametara kao što su Kirijeva konstanta, Kirijeva temperatura i parametar γ koji opisuje difuzivnost i stepen nelinearnosti promene ε_r od temperature iznad Kirijeve temperature.**

***Ključne reči* – $BaTiO_3$, Pechini metoda, dielektrična konstanta.**

I. Uvod

U cilju istraživanja i razvijanja novih elektronskih materijala, velika pažnja se posvećuje proučavanju konsolidacije barijum-titanatne ($BaTiO_3$) keramike. Karakteristike keramike na bazi $BaTiO_3$, kao što su velika kapacitivnost, pozistorski i varistorski efekti, otvaraju mogućnost razvijanja različitih tipova elektronskih komponenata. Pri tome, promenom sastava i dodavanjem primesa polaznom materijalu, kao i kontrolisanjem uslova dobijanja, mogu nastati različiti tipovi poluprovodničke keramike. Neke od mogućih primena su kod termistora sa visokim vrednostima pozitivnog temperaturnog koeficijenta (PTC) otpornosti, optoelektronskih elemenata, višeslojnih kondenzatora, dinamičkih memorija sa slučajnim pristupom (DRAM) u integrisanim kolima, kao i u sistemima za konverziju energije [1, 2]. Električna svojstva polikristalnih materijala zavise od mikrostrukturnih konstituenata, pre svega od metode koja je korišćena za sintezu početnih prahova, postupka sinterovanja, gustine, poroznosti, kao i od raspodele i veličine zrna i pora.

Prisustvo poroznosti utiče na smanjenje dielektrične konstante i povećava dielektrične gubitke [3]. Takođe, usled prisustva poroznosti, smanjuje se čvrstoća keramičkog materijala. Ispitivanja su pokazala da se usled povećanja temperature sinterovanja, povećava i gustina i veličina zrna porozne keramike, dok poroznost opada [4]. Utvrđeno je i da relativna propustljivost raste usled smanjenja poroznosti materijala. Tako se kontrolom poroznosti može dobiti keramika sa velikom dielektričnom konstantom i malim dielektričnim gubitkom [4].

Poznato je da električna svojstva, pre svega PTC efekat, u velikoj meri zavise od rasta zrna tokom sinterovanja, kao i od vrste i koncentracije donorskih ili akceptorskih primesa. Dopanti koji se dodaju barijum-titanatnoj keramici imaju ulogu da prilagode električna i poluprovodnička svojstva prema zahtevima elektronskih komponenata [5, 6]. Takođe, električne karakteristike u mnogome zavise od afiniteta jona dopanata prema određenoj poziciji u $BaTiO_3$ rešetki.

Usled nesavršenosti rešetke barijum-titanata (koji ima perovskitnu strukturu), postoji veliki broj mogućnosti jonskih zamena u strukturnim rešetkama. To direktno utiče na dielektrična i poluprovodnička svojstva ovakvih materijala. Joni sa većim jonskim radijusom pretenduju da zauzmu mesto Ba^{2+} u perovskitnoj strukturi, pri čemu je poželjno da to budu joni retkih zemalja. Takvi su na primer trovalentni katjoni Yb^{3+}, Er^{3+}, Ho^{3+}, Dy^{3+}. Ovakva supstitucija zahteva formiranje negativno naelektrisanih defekata, kako bi se očuvala elektroneutralnost [7-9]. Sa druge strane, joni sa manjim jonskim radijusom, kao što je Nb^{5+}, pretenduju da zauzmu mesto Ti^{4+} u perovskitnoj strukturi. Ukoliko je, pri supstituciji Ba^{2+}, koncentracija aditiva, npr. La, niska (ispod 0.5 at%), dolazi do formiranja čvrstih rastvora. U suprotnom slučaju, ukoliko je koncentracija aditiva viša (iznad 0.5 at%), nezavisno da li se radi o supstituciji Ba^{2+} ili Ti^{4+} jona, uočen je porast specifične električne otpornosti uzorka, reda veličine 10^8 Ωm [9].

Sandra Veljković - Univerzitet u Nišu, Elektronski fakultet, Aleksandra Medvedeva 14, 18000 Niš, Srbija (e-mail: sandra.veljkovic@elfak.rs).
Miloš Đorđević – Univerzitet u Nišu, Elektronski fakultet, Aleksandra Medvedeva 14, 18000 Niš, Srbija (e-mail: milos.djordjevic@elfak.ni.ac.rs).
Vesna Paunović – Univerzitet u Nišu, Elektronski fakultet, Aleksandra Medvedeva 14, 18000 Niš, Srbija (e-mail: vesna.paunovic@elfak.ni.ac.rs).
Zoran Prijić – Univerzitet u Nišu, Elektronski fakultet, Aleksandra Medvedeva 14, 18000 Niš, Srbija (e-mail: zoran.prijic@elfak.ni.ac.rs).
Vojislav Mitić – Univerzitet u Nišu, Elektronski fakultet, Aleksandra Medvedeva 14, 18000 Niš, Srbija (e-mail: vojislav.mitic@elfak.ni.ac.rs).

Još jedan od razloga korišćenja modifikovane barijum-titanatne keramike je i taj da aditivi utiču na pomeranje Kirijeve temperature, odnosno na smanjenje njene vrednosti [4].

U ovom radu ispitivana su mikrostrukturna svojstva $BaTiO_3$ keramike čiji su početni prahovi dobijeni različitim metodama. Takođe ispitivan je i uticaj tako dobijene mikrostrukture i dopiranja na električna svojstva $BaTiO_3$ keramike.

II. Eksperimentalni deo

A. Pechini metoda

Uzorci La/Mn dopirane $BaTiO_3$ keramike pripremljeni su iz citratnih rastvora Ti, La, Mn i Ba actetata, odnosno od njihovih organo-metalnih kompleksa primenom modifikovane Pechini metode [10]. Ova metoda omogućava sintezu praha na niskim temperaturama (ispod 800°C), dobru stehiometriju i laku ugradnju dopanata u kristalnu rešetku. Koncentracija dodatog oksida, La_2O_3, bila je 0.5 at%, dok je koncentracija MnO_2 bila 0.05 at% u svim uzorcima. Poređenja radi, uzorci bez La i Mn pripremljeni su na isti način. Modifikovani Pechini postupak je izveden kao trofazni postupak za pripremu prekursora. Detaljni postupak sinteze je ranije opisan u radovima [10,11]. Nakon kalcinacije na 700°C, prah je mleven i presovan pri pritisku od 100MPa u pelete prečnika 10 mm i debljine 2 mm. Uzorci su potom sinterovani u atmosferi vazduha na temperaturi od 1310°C tokom 2 sata, a brzina zagrevanja je bila 10°C/min. Zapreminska gustina merena je Arhimedovom metodom.

B. Konvencionalna metoda

Uzorci La/Mn dopirane keramike korišćeni u ovom istraživanju dobijeni su iz komercijalnog $BaTiO_3$ praha, ELMIC BT 100 Rhone Poulenc: veličine čestica 0,1 μm - 0,7 μm. Stehiometrijski odnos BaO/TiO_2 bio je 0,996 ± 0,004. La_2O_3 (Merck, Darmstadt) je korišćen kao donorski dopant. Koncentracija donora bila je 0.5 at% kao i kod Pechini metode. MnO_2 sa koncentracijom od 0.05 at%, korišćen je kao akceptor. Praškovi su mleveni sa Al_2O_3 kuglicama u suspenziji etil-alkohola. Vreme homogenizacije i mlevenja je 24h. Praškovi su zatim sušeni na 200°C nekoliko sati i izostatski presovani na 100 MPa u tablete (pelete) cilindričnog oblika, prečnika 10 mm (Hidraulic Press VPM VEB - Thuringer Industrieverg Raunestein). Pripremljene tablete sinterovane su u laboratorijskoj peći (Lenton Thermal Design LTD) na 1310°C u keramičkim posudama. Sinterovanje je sprovedeno u atmosferi vazduha tokom 2 sata. Režim zagrevanja je bio 5°C/min do temperature od 850°C, a zatim od 12°C/min do željene temperature sinterovanja. Brzina hlađenja je bila 10°C/min do sobne temperature. Arhimedov metod je korišćen za merenje gustine.

Skenirajući elektronski mikroskop (JSM-5300), opremljen energetsko disperzivnim spektrometrom (EDS-QX 2000S system), korišćen je za ispitivanje mikrostrukture uzoraka dobijenih posle sinterovanja. Uzorci su prekriveni Au elektrodama da bi se poboljšala provodljivost tokom merenja. Kapacitivnost i tangens ugla gubitka sinterovanih uzoraka mereni su pomoću LCR-metra Agilent 4284A u frekventnom opsegu između 100 Hz i 20 kHz. Relativna dielektrična konstanta izračunata je iz izmerenih kapacitivnosti. Temperaturni interval u kome je izmerena dielektrična konstanta je od 20°C do 180°C. Dielektrični parametri kao što su Kirijeva temperatura (T_C), Kiri-Vajsova temperatura (T_0), Kirijeva konstanta (C), zajedno sa kritičnim eksponentom nelinearnosti γ izračunate su korišćenjem Kiri-Vajsovog i modifikovanog Kiri-Vajsovog zakona.

III. Rezultati i diskusija

A. Mikrostrukturna svojstva

Za gustinu uzoraka nedopirane $BaTiO_3$ keramike karakteristično je da se kretala od 80% teorijske gustine (TG) za keramiku dobijenu konvencionalnom metodom do 85% TG za keramiku dobijenu Pechini metodom. Kod uzoraka dopiranih La/Mn zabeležena je veća gustina i ona se kretala od 90 do 95% TG pri čemu je, kao i kod nedopiranih uzoraka, veća gustina zabeležena kod La/Mn dopiranih uzoraka dobijenih Pechini metodom.

Mikrostrukturne karakteristike nedopirane $BaTIO_3$ keramike prikazane su na Sl. 1 i Sl. 2. Za uzorke $BaTiO_3$ dobijene konvencionalnom metodom karakterističan je diskontinualni rast zrna i veličina zrna od 3 do 15 μm (Sl. 1).

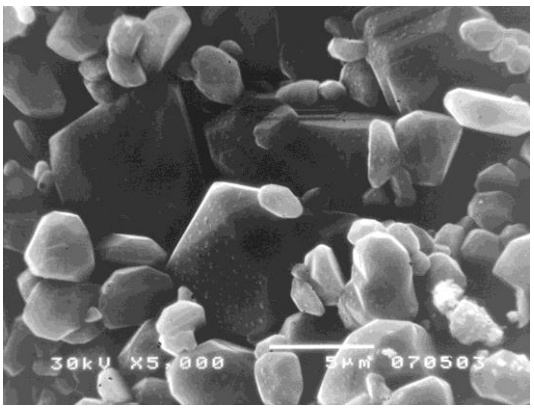

Sl. 1. SEM mikrostruktura nedopiranog $BaTiO_3$ dobijenog konvencionalnom metodom.

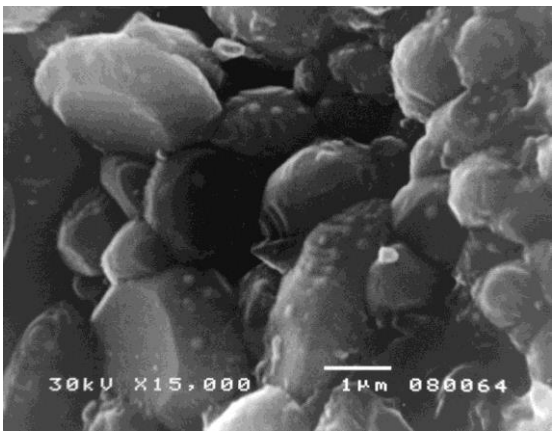

Sl. 2. SEM mikrostruktura nedopiranog $BaTiO_3$ dobijenog Pechini metodom.

Kod uzoraka nedopiranog $BaTiO_3$ dobijenog Pechini metodom (Sl. 2) karakteristična je sitnija mikrostruktura i srednja veličina zrna koja se kretala u opsegu od 1-10 µm.

Glavna karakteristika uzoraka La/Mn-$BaTiO_3$ keramike dobijene konvencionalnom metodom je uniformna sitnozrnasta mikrostruktura sa normalnim rastom zrna i veličinom zrna koja se kretala od 0.5 do 2 µm (Sl. 3).

Mikrostruktura La/Mn-$BaTiO_3$ keramike dobijene Pechini metodom data je na Sl. 4. Za La/Mn-$BaTiO_3$ keramiku dobijenu Pechini metodom karakteristična je bimodalna mikrostruktura i postojanje dve oblasti koje se razlikuju po obliku i veličini zrna. Nasuprot sitnozrne matrice sa poligonalnim zrnima veličine od 1-2 µm, postoje i lokalna područja sa sekundarnim abnormalnim zrnima nepravilnog oblika i veličinom zrna do 10 µm (Sl. 4).

EDS analize La/Mn dopiranih uzoraka dobijenih konvencionalnom metodom, uzete iz različitih područja istog uzorka, pokazale su postojanje oblasti sa povećanim sadržajem La što je ukazalo na neuniformnu raspodelu dopanata (Sl. 5).

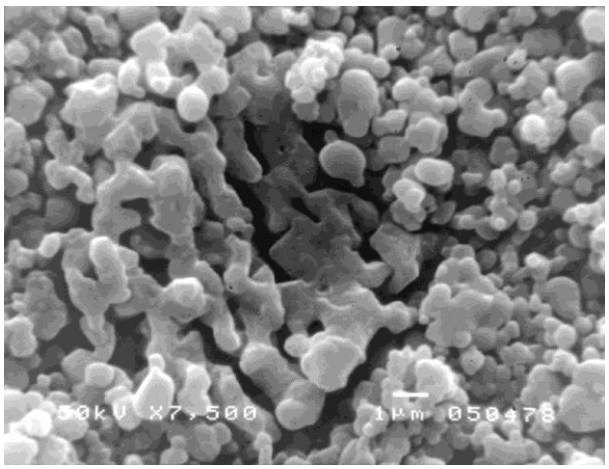

Sl. 3. SEM mikrostruktura La/Mn-$BaTiO_3$ dobijenog konvencionalnom metodom.

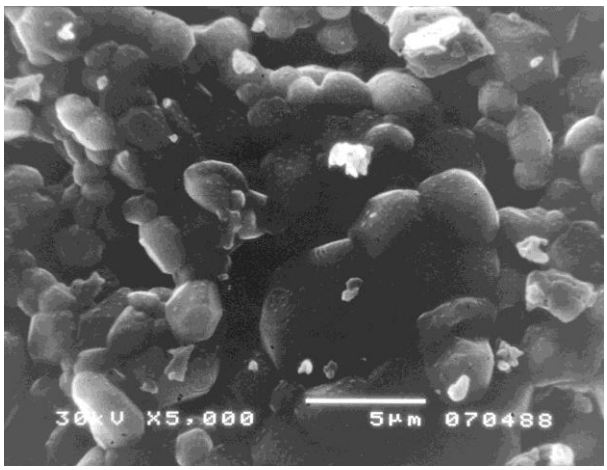

Sl. 4. SEM mikrostruktura La/Mn-$BaTiO_3$ dobijenog Pechini metodom.

Postojanje pika X-zračenja za lantan (Lα-La) na EDS spektru ukazuje da regioni bogati La postoje istovremeno sa nominalnom perovskitnom fazom $BaTiO_3$.

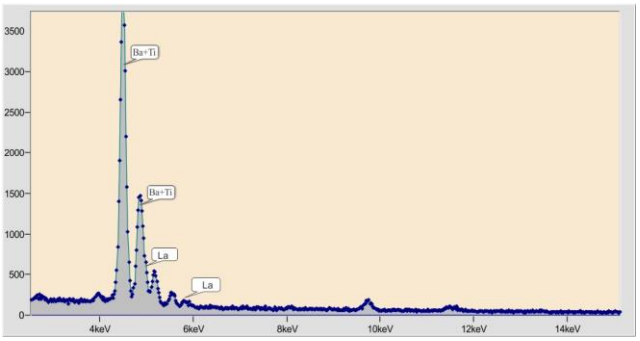

Sl. 5 EDS spektar La/Mn dopirane $BaTiO_3$ keramike dobijene konvencionalnom metodom.

Za razliku od ovih uzoraka, EDS analiza uzoraka dobijenih Pechini metodom, nije pokazivali pikove La i Mn što ukazuje na homogenu raspodelu donorskih i akceptorskih primesa i vodi ka keramici sa visokim vrednostima dielektrične konstante.

B. Električna svojstva

Električne karakteristike dopirane i nedopirane $BaTiO_3$ keramike dobijene različitim metodama ispitivane se kroz promenu dielektrične konstante sa frekvencijom i temperaturom. Frekventni opseg za sve ispitivane uzorke kretao se od 100 Hz do 20 kHz. Zavisnost dielektrične konstante u funkciji frekvencije data je na Sl. 6. U slučaju nedopirane keramike može se videti da je tok promene dielektrične konstante sa frekvencijom isti u oba slučaja sa tim što je kod uzoraka dobijenih Pechini metodom vrednost dielektrične konstante nešto veća nego kod uzoraka dobijenih konvencionalnom metodom. Ovakve vrednosti su direktna posledica veće gustine uzoraka dobijenih Pechini metodom kao i uniformnije mikrostrukture kod ovih uzoraka.

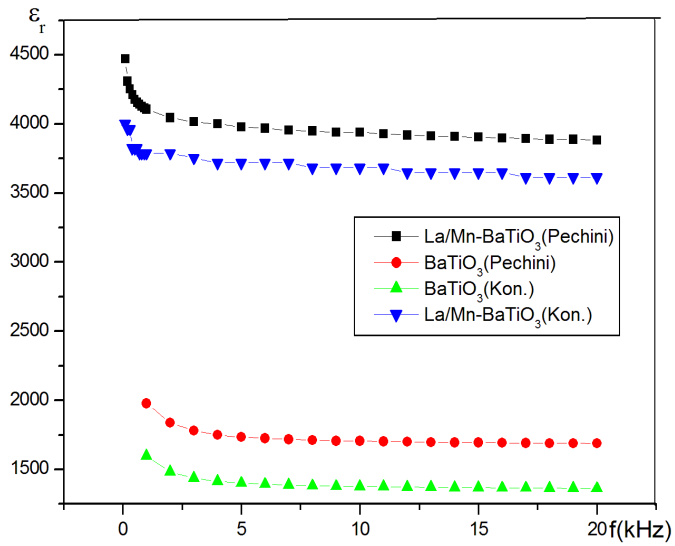

Sl. 6. Zavisnost dielektrične konstante od frekvencije.

U slučaju dopirane keramike za obe metode procesiranja početnih prahova dobijaju se znatno veće vrednosti dielektrične konstante u odnosu na nedopiranu keramiku. Takođe može se primetiti da su više vrednosti dielektrične konstante primećene kod uzoraka dobijenih Pechini metodom. Najveća vrednost dielektrične konstante na sobnoj temperaturi na 100 Hz iznosi 4500 i to kod La/Mn-$BaTiO_3$ dopirane keramike dobijene Pechini metodom. Ove uzorke karakteriše bimodalna mikrostruktura, homogeni sastav kao i najveća gustina. Dielektrična konstanta za sve ispitivane uzorke posle početnih visokih vrednosti na nižim frekvencijama opada sa porastom frekvencije i postiže konstantnu vrednost za f >5 kHz

Uticaj sinteze prahova i dopiranja na dielektrične karakteristike $BaTiO_3$ keramike ispitivan je preko zavisnosti dielektrične konstante ε_r od temperature (Sl. 7). Kao i kod uticaja frekvencije na ε_r i ovde su zabeležene veće vrednosti dielektrične konstante kod donor akceptor dopiranih uzoraka. Na osnovu krivih zavisnosti dielektrične konstante od temperature može se videti da najvišu vrednost dielektrične konstante na Kirijevoj temperaturi ε_r=7837 kao i najveću promenu sa temperaturom pokazuju La/Mn-$BaTiO_3$ uzorci dobijeni Pechini metodom. Niže vrednosti dielektrične konstante kod uzoraka dobijenih konvencionalnom metodom posledica su sa jedne strane manje relativne gustine ovih uzoraka i sa druge strane nehomogene mikrostrukture. Kod uzoraka nedopirane $BaTiO_3$ keramike dobijenih konvencionalnom metodom kriva promena dielektrične konstante sa temperaturom nema tako izraženi maksimum kao što je slučaj sa dopiranim uzorcima i uzorkom čistog $BaTiO_3$ dobijenog Pechini metodom. Maksimalna vrednost ε_r kod ovih uzoraka je 3491 za razliku od ε_r vrednosti kod uzoraka dobijenih Pechini metodom gde je ε_r=5488. Više vrednosti dielektrične konstante kod nedopiranih uzoraka dobijene Pechini metodom, proizilaze iz činjenice da ovi uzorci imaju bolju homogenost mikrostrukture i veću relativnu gustinu.

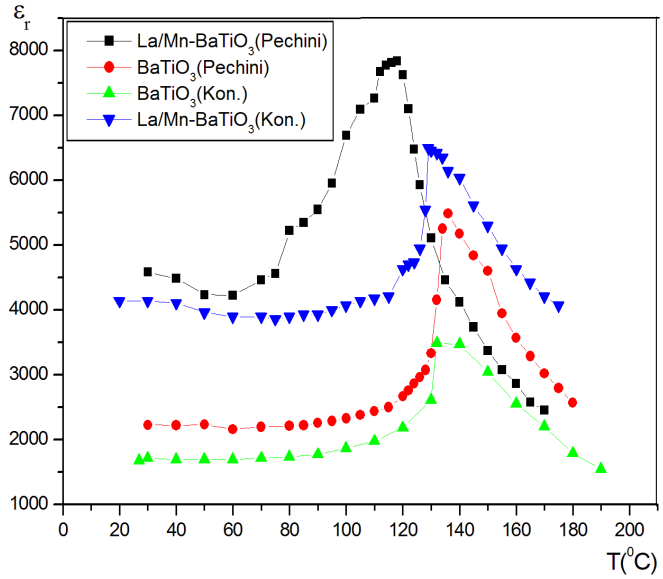

Sl. 7. Zavisnost dielektrične konstante od temperature.

Za sve ispitivane uzorke došlo je do pomeranja Kirijeve temperature (T_C) ka nižim vrednostima u odnosu na Kirijevu temperaturu nedopirane keramike dobijene konvencionalnom metodom koja iznosi 132°C. Najniža vrednost T_C zabeležena je kod La/Mn-$BaTiO_3$ keramike dobijene Pechini metodom i iznosi 118°C.

Više vrednosti dielektrične konstante u keramici sa donorskim (La) i akceptorskim (Mn) primesama mogu se pripisati smanjenju koncentracije kiseoničnih vakancija u odnosu na nedopiranu keramiku, čime se povećava gustina keramike i dobija se keramika sa visokim vrednostima dielektrične konstante.

Za sve ispitivane uzorke, bez obzira na način dobijanja, karakterističan je oštar prelaz iz feroelektrične u paraelektričnu fazu na Kirijevoj temperaturi. Ovo se može potvrditi odnosom dielektrične konstante na Kirijevoj temperaturi (ε_{rmax}) i na sobnoj temperaturi (ε_{rmin}), tj. ($\varepsilon_{rmax}/\varepsilon_{rmin}$). Kao što se iz Tabele 1 može videti, najveća vrednost odnosa dielektričnih konstanti ($\varepsilon_{rmax}/\varepsilon_{rmin}$=1.7) izračunat je kod uzoraka La/Mn-$BaTiO_3$ dobijenih Pechini metodom.

Fitovanjem krivih koje predstavljaju zavisnosti recipročne vrednosti dielektrične konstante od temperature (Sl. 8) izračunate su vrednosti Kirijeve konstante (C) za sve ispitivane uzorke (Tabela 1). Najvišu vrednost Kirijeve konstante ima La/Mn-$BaTiO_3$ keramika dobijena konvencionalnom metodom (C=3.38·10^5 K) a najnižu nedopirana keramika dobijena konvencionalnom metodom (C=7.76·10^4 K). Vrednosti za Kirijevu konstantu su u saglasnosti sa promenom gustine ispitivanih uzoraka kao i sa mikrostrukturnim karakteristikama.

Za Kiri–Vajsovu temperaturu (T_0) su karakteristične niže vrednosti u odnosu na Kirijevu temperaturu (T_C) za sve ispitivane uzorke (Tabela 1).

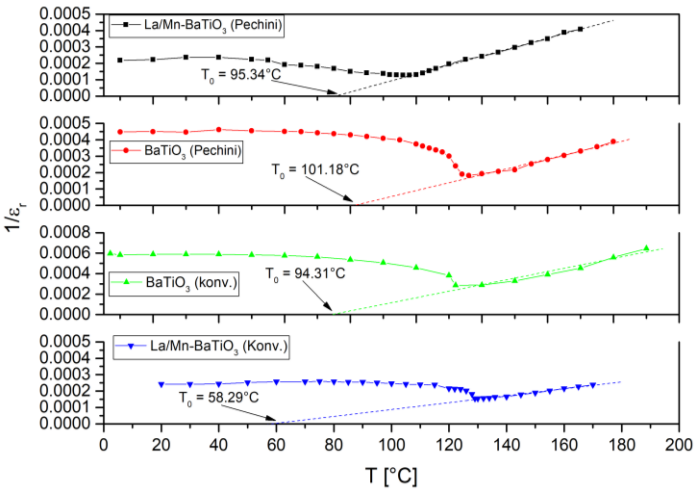

Sl. 8 Recipročna vrednost dielektrične konstante u funkciji temperature.

Kritični eksponent nelinearnosti γ izračunat je fitovanjem krive $ln(1/\varepsilon_r-1/\varepsilon_{rmax})$ u funkciji od $ln(T-T_{max})$, gde T_{max} predstavlja temperaturu na kojoj je vrednost ε_r maksimalna, i

predstavlja nagib te krive (Sl. 9).

TABELA I
DIELEKTRIČNI PARAMETRI ZA ISPITIVANE UZORKE

Uzorci	ε_r na T=300K	ε_r na T_C	T_c [°C]	T_0 [°C]	C [K] $\cdot 10^4$	γ
$BaTiO_3$ –kon.	1680	3491	132	94	7.67	1.38
BT –Pechini	2230	5488	130	101	8.65	1.32
La/Mn-BT – kon.	4140	6491	126	58	33.8	1.47
La/Mn-BT – Pechini	4500	7837	118	95	20.4	1.05

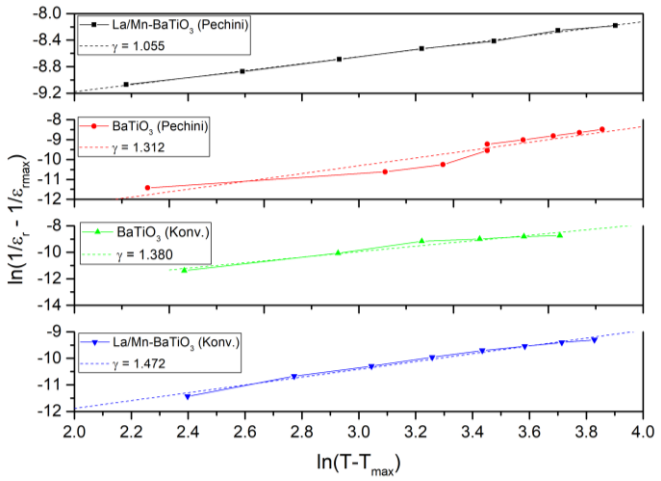

Sl. 9. Zavisnost $\ln(1/\varepsilon_r-1/\varepsilon_{rmax})$ od $\ln(T-T_{max})$

Za ispitivane uzorke $BaTiO_3$ vrednost kritičnog eksponenta γ kretala se od 1.05 do 1.47 što je u skladu sa eksperimentalnim podacima jer je za ove uzorke karakterističan oštar prelaz iz feroelektrične u paraelektričnu oblast. Najizrazitija promena iz feroelektrične u paraelektričnu oblast zapažena je kod La/Mn-$BaTiO_3$ dobijenog Pechini metodom za koju je γ=1.05.

IV. ZAKLJUČAK

U ovom radu ispitivan je uticaj početnih prahova dobijenih različitim metodama na mikrostrukturne i dielektrične karakteristike nedopirane i La/Mn dopirane $BaTiO_3$ keramike. SEM/EDS ispitivanja su pokazala da je za keramiku dobijenu Pechini metodom karakteristična sitnozrna i homogena mikrostruktura kao i homogeni kompozicioni sastav bez pikova La i Mn. Ovakva mikrostruktura dovela je do viših vrednosti dielektrične konstante. Najvišu vrednost dielektrične konstante na Kirijevoj temperaturi ε_r=7837 kao i najveću promenu sa temperaturom pokazala je La/Mn-$BaTiO_3$ keramika dobijena Pechini metodom. Kod svih ispitivanih uzoraka došlo je do pomeranja Kirijeve temperature ka nižim vrednostima u odnosu na Kirijevu temperaturu nedopirane keramike. Na osnovu Kiri–Vajsovog zakona izračunati su parametri poput Kiri-Vajsove temperature (T_0) i Kirijeve konstante (C). Najviša vrednost Kirijeve konstante izračunata je kod La/Mn-$BaTiO_3$ keramike dobijene konvencionalnom metodom (C=3.38·10^5 K), a najniža za nedopiranu keramiku dobijenu konvencionalnom metodom (C=7.76·10^4 K). Kritični eksponent nelinearnosti γ kretao se u opsegu od 1.05 do 1.47 što je u skladu sa eksperimentalnim podacima jer je za sve uzorke karakterističan oštar prelaz iz feroelektrične u paraelektričnu oblast.

ZAHVALNICA

Ovaj rad je finansiran od strane Ministarstva prosvete, nauke i tehnološkog razvoja Republike Srbije na čemu se autori iskreno zahvaljuju.

LITERATURA

[1] C. Pithan, D. Hennings, R. Waser, "Progress in the Synthesis of Nanocrystalline $BaTiO_3$ Powders for MLCC", *Int. J. Appl. Ceram. Tech.*, vol. 2, no. 1, pp. 1–14, 2005.
[2] D.H. Kuo, C.H.Wang, W.P.Tsai, "Donor and acceptor cosupstitued BaTiO3 for nonreducible multilayer ceramic capacitors", *Ceram. Int.* vol. 32, pp. 1-5, 2006.
[3] H.I. Hsiang, F. S. Yen, C. Y. Huang, "Effects of porosity on dielectric properties of $BaTiO_3$ ceramics", *Jpn. J. Appl. Phys.*, vol. 34, pp. 1922–1925, 1995.
[4] V. Paunovic, V. V. Mitic, Lj. Kocic, "Dielectric characteristics of donor-acceptor modified $BaTiO_3$ ceramics", *Ceram. Int.* vol. 42, no. 10, pp. 11692-11699, 2016.
[5] W. Caia, C. Fu, Z. Lin, X. Deng, W. Jiang, "Influence of Lanthanum on Microstructure and Dielectric Properties of Barium Titanate Ceramics by Solid State Reaction", *Advanced Materials Research*, vol. 412 pp. 275-279, 2012
[6] A. Ianculescu, Z.V. Mocanu, L.P. Curecheriu, L. Mitoseriu, L. Padurariu, R. Trusca, "Dielectric and Tunability Properties of La-doped $BaTiO_3$ ceramics", *Journal of Alloys and Compounds*, vol. 509, Issue 41, pp. 10040–10049, 2011.
[7] V. Paunovic, V. V. Mitic, M. Đorđević, M. Marjanović, Lj. Kocic, "Electrical Characteristics of Er Doped $BaTiO_3$ Ceramics", *Sci. Sinter.*, vol. 49, no. 2, pp. 129-137, 2017.
[8] V. Paunovic, V. V. Mitic, M. Miljkovic, V. Pavlovic, Lj. Živkovic, "Ho_2O_3 Additive Effects on $BaTiO_3$ Ceramics Microstructure and Dielectric Properties" *Sci. Sinter.*, vol. 44, no. 2, pp. 223-233, 2012.
[9] M. Đorđevic, M. Marjanovic, V. Paunovic, V. MItic, Z. Prijic, "Električne karakteristike i fazna transformacija Yb dopirane $BaTiO_3$ keramike", ETRAN, Silver lake, Serbia, Proceedings 59th Conference ETRAN, pp. NM 1.1, jun 2015.
[10] M. P. Pechini, Method of preparing lead and alkaline earth titanates and coating method using the same to form a capacitor, *US Patent No.* 3.330.697, 1967.
[11] Vesna Paunović, Zoran Prijić, Miloš Đorđević, Vojislav Mitić, Enhanced dielectric properties in La modified barium titanate ceramics, Facta Universitatis, Series: Electronics and Energetics, University of Niš, Vol. 32, No 2, June 2019, pp. 179-193

ABSTRACT

In this paper, the microstructural and dielectric properties of pure and La/Mn doped $BaTiO_3$, whose initial powders were obtained by different methods, were investigated. The methods for obtaining the initial powders were the conventional method of preparation starting from pure oxides and the Pechini method starting from the organic-

metal complex as a precursor. The systems were sintered at 1310°C for two hours. The analysis of the microstructure of undoped $BaTiO_3$ ceramics showed that the ceramics obtained by the conventional method are characterized by a discontinuous grain growth and grain size of 3 to 15 µm, while the samples obtained by the Pechini method are characterized by a uniform microstructure and grains of 1 to 10 µm. The La/Mn doped ceramics obtained by the Pechini method are characterized by a bimodal microstructure and a homogeneous distribution of additives. The dielectric constant was tested in the frequency range from 100 Hz to 20 kHz. The highest value and change of dielectric constant with temperature was shown by La/Mn doped $BaTiO_3$ ceramics obtained by the Pechini method. The dielectric constant of this ceramic at the Kiri temperature was 7837. The Curie-Weiss law and the modified Curie-Weiss law were used to calculate parameters such as the Curie constant, the Curie temperature, and the parameter γ which describes the diffusivity and degree of nonlinearity of the change ε_r from the temperature above the Curie temperature.

Influence of initial powder synthesis on microstructural and electrical properties of $BaTiO_3$ ceramics

Sandra Veljković, Miloš Đorđević, Vesna Paunović, Zoran Prijić, Vojislav Mitić

Karakterizacija dopirane $BaTiO_3$ keramike primenom nove metode za merenje električnih karakteristika

Miloš Đorđević, *Student Member, IEEE,* Miloš Marjanović, *Student Member, IEEE,* Vesna Paunović, *Member, IEEE,* Danijel Danković, *Member, IEEE*

***Apstrakt* - U ovom radu je opisano poređenje eksperimentalnih rezultata dobijenih manuelnim putem i primenom nove metode za merenje i karakterizaciju dopirane $BaTiO_3$ keramike na različitim temperaturama i frekvencijama. Za merenje i karakterizaciju parametara materijala u funkciji temperature korišćeni su LCR metar i programabilna peć za testiranje. Rezultati dobijeni manuelnom kontrolom LCR metra su mereni ručnim zadavanjem parametara. Dobijeni rezultati su poređeni sa rezultatima dobijenih primenom nove metode za automatsku kontrolu LCR metra, za koju je razvijena aplikacija. Na osnovu toga pokazano je da se merenje karakteristika može obaviti potpuno automatizovano. Rezultati koji su poređeni su dobijeni merenjem uzoraka dopirane Nb/$BaTiO_3$ keramike. Na osnovu analize izmerenih rezultata može se zaključiti da je nova metoda preciznija i sa rezultatima je lakše manipulisati u daljem radu.**

Ključne reči - $BaTiO_3$ keramika; aplikacija; električne karakteristike.

I. Uvod

Dopirana $BaTiO_3$ pripada najčešće ispitivanim keramikama zbog svojih feroelektričnih osobina. Barijum titanat ima relativno nisku Kirijevu temperaturu (120°-130°C). Ovo omogućava maksimalnu vrednost dielektrične konstante u temperaturnom opsegu u kome se ova osobina najefikasnije može koristiti. Na osnovu toga, poznato je da se veliki broj elektronskih komponenti izrađuje na bazi $BaTiO_3$ keramike, kao što su PTC termistori, višeslojni kondenzatori, piezoelektrični senzori, komunikacioni filtri, itd [1-2]. Kako bi se dobili što validniji podaci o ispitivanoj keramici, neophodno je precizno izmeriti određene parametre ispitivanih uzoraka.

Kao što je poznato, dielektrična ili poluprovodna svojstva $BaTiO_3$ keramike su uslovljena dopanatima koji mogu zauzimati mesta Ba^{2+} ili Ti^{4+} jona, što zavisi od radijusa jona koji se ugrađuju.

Kako su radijusi jona trovalentnih katjona retkih zemalja kao što su Yb^{3+}, Er^{3+}, Dy^{3+} po veličini između jonskih radijusa Ba^{2+} ili Ti^{4+} jona, joni dopanata mogu da zauzmu A ili B položaje u perovskitnoj strukturi $BaTiO_3$ keramike [3,4].

Miloš Đorđević – Univerzitet u Nišu, Elektronski fakultet, Aleksandra Medvedeva 14, 18000 Niš, Srbija (email: milos.djordjevic@elfak.ni.ac.rs).

Miloš Marjanović- Univerzitet u Nišu, Elektronski fakultet, Aleksandra Medvedeva 14, 18000 Niš, Srbija (email: milos.marjanovic@elfak.ni.ac.rs).

Vesna Paunović – Univerzitet u Nišu, Elektronski fakultet, Aleksandra Medvedeva 14, 18000 Niš, Srbija (email: vesna.paunovic@elfak.ni.ac.rs).

Danijel Danković – Univerzitet u Nišu, Elektronski fakultet, Aleksandra Medvedeva 14, 18000 Niš, Srbija (email: danijel.dankovic@elfak.ni.ac.rs).

Na osnovu dopanata koji se dodaju $BaTiO_3$ keramici dolazi do pomeranja Kirijeve temperature, koja utiče na električna svojstva dopirane keramike. Kako bi se odredila električna svojstva dopirane keramike, potrebno je precizno izmeriti parametre kao što su dielektrična konstanta, dielektrični gubici, otpornost ispitivanih uzoraka, na osnovu kojih je moguće odrediti druge parametre poput specifične električne otpornosti [5,6]. Na validnost izmerenih vrednosti utiče način merenja, odnosno zadavanja parametara i kontrole samog merenja.

U ranijim istraživanjima [7] ispitivali smo primenu virtuelne instrumentacije za automatizaciju merenja i karakterizacije električnih materijala. Prednost nove metode koja je opisana u ovom radu u odnosu na ranija merenja, ogleda se u mogućnosti praćenja rezultata tokom merenja u vidu dinamičke tabele, odnosno tabelarnog prikaza koji se ažurira svakim novim korakom u toku merenja.

Virtuelna instrumentacija sve više preuzima vodeću ulogu kako u laboratorijama tako i u industriji. Postoji sve veća potreba za virtuelnom instrumentacijom pri upotrebi instrumenata koji ne poseduju svoj operativni sistem, pa je nemoguće kontrolisati njihov rad. Takođe, postoji potreba za virtuelnom instrumentacijom ako je neophodno koristiti više instrumenata za obavljanje testa i praćenje parametara tokom testa u isto vreme. Virtuelna instrumentacija koja podrazumeva primenu više instrumenata istovremeno, često znači i potrebu za objedinjavanje više različitih komunikacionih protokola. Na ovaj način je moguće povezati nekoliko instrumenata čiji se rad kontroliše, a samim tim instrumenti šalju izmerene podatke najčešće računaru, gde je moguće pratiti izmerene parametre i čuvati ih.

Za realizaciju virtuelne instrumentacije kao komunikacioni protokol često se koristi serijska komunikacija zasnovana na RS-232 ili USB standardu ili paralelna komunikacija zasnovana na GPIB standardima (poznatiji kao HP-IB, IEEE 488.1-2 ili IEC 625.1-2), PC bus ili VXI magistrala (VME eXtension for Instrumentation). Osnovne kategorije virtuelne instrumenatacije mogu se podeliti na sledeći način:

1. Softverska aplikacija za kontrolu modula ili instrumenata kao što su: DAK ploča (eng. *DAK board*), kontrolisani instrument zasnovan na GPIB ploči, kontrolisani instrument povezan preko serijskog porta (RS-232), kontrolisani instrument sa VXI pločom (ili sistem).

2. Grafički prednji panel (eng. *Graphic front panel*) bez fizičkih instrumenata spojenih na računar. Umesto toga,

računar dobija i analizira podatke iz datoteka ili sa drugih računara na mreži, ili čak može matematički izračunati svoje podatke da simulira fizički proces ili događaj, da ne zahteva obavezno merenje i prikupljanje realnih podataka iz stvarnog sveta. Na računar su u skladu sa tačkom (1) priključeni sledeći procesni merni uređaji: Senzori, GPIB instrumenti, Serijski instrumenti.

U ovom radu biće predstavljeno poređenje eksperimentalnih rezultata dopirane Nb-$BaTiO_3$ dobijenih manuelnom kontrolom i primenom nove metode za automatsku kontrolu LCR metra.

II. Eksperimentalni deo

Uzorci Nb dopirane $BaTiO_3$ keramike dobijeni su konvencionalnom metodom sinterovanja u čvrstoj fazi polazeći od čistih oksidnih prahova $BaTiO_3$ (Rhone Poulenc Ba/Ti=0.996±0.004) i Nb_2O_3 (Fluka chemika). Početni prahovi su mešani u izopropil alkoholu, a zatim sušeni i presovani u pelete prečnika 7 mm i debljine 2 mm na pritisku od 120 MPa. Nakon presovanja, vršeno je sinterovanje uzoraka u atmosferi vazduha na temperaturi 1300°C u trajanju od 2 sata.

Pre merenja dielektričnih karakteristika na uzorke je naneta srebrna pasta u svrhu formiranja električnih kontakata. Dielektrične karakteristike merene su pomoću LCR-metra Agilent 4284A u frekventnom opsegu od 100 Hz do 1 MHz i u opsegu temperatura od 20°C do 180°C.

III. Tehnike kontrole i merenja

Uzorci Nb dopirane $BaTiO_3$ ispitivani su na različitim temperaturama i frekvencijama primenom manuelne kontrole i primenom nove metode za automatsku kontrolu LCR metra.

A. Manuelna kontrola

Manuelno ispitivanje uzoraka $BaTiO_3$ keramike se sastojalo u tome da se uzorci uneti u peć postepeno zagrevaju i na tačno određenim temperaturama (što je preciznije moguće bilo) ručno pokrene merenje LCR metra. S druge strane, neophodno je bilo u što kraćem roku izvršiti merenje parametara na jednoj vrednosti temperature, ali na različitim frekvencijama (100 Hz do 1 MHz). Takođe je zapisivanje vrednosti trebalo vršiti što preciznije, kako bi merenje bilo validno.

B. Nova metoda za automatsku kontrolu LCR metra

Princip rada metode je zasnovan na 4 osnovna bloka, kao što se može videti na slici 1.

Kako bi merenje uzoraka bilo što tačnije i preciznije, razvijena je aplikacija kojom je vršena automatska kontrola LCR metra (Sl. 2). Primenom nove metode ispitivani su dopirani uzorci $BaTiO_3$ keramike, na različitim temperaturama i frekvencijama. Za razliku od manuelne kontrole, ovde je olakšana kontrola kao i merenje ispitivanih uzoraka. U okviru aplikacije zadati su parametri koji se prate tokom testa, kao i temperaturni i frekventni opseg (sa unapred definisanim korakom merenja) u okviru kog se vrši merenje.

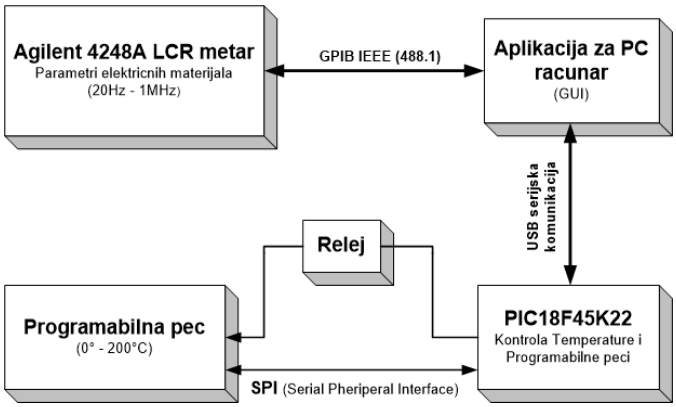

Sl. 1. Blok dijagram sistema za merenje

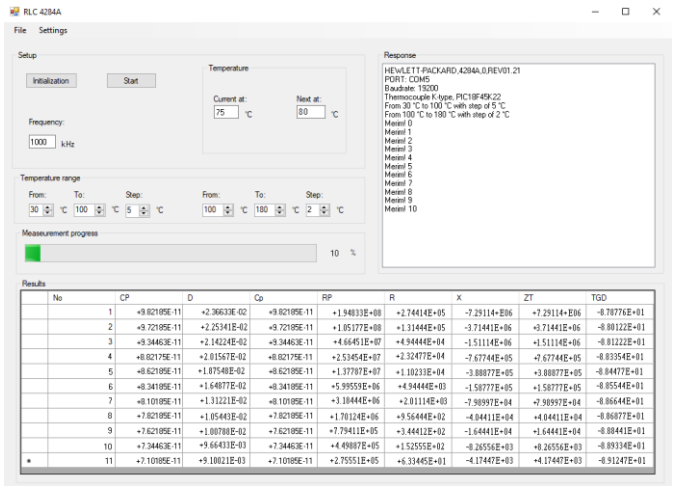

Sl. 2. Izgled grafičkog korisničkog interfejsa aplikacije (*GUI – Graphical User Interface*)

Izmerene vrednosti se mogu pratiti u tabeli koja je deo same aplikacije, kako bi korisnik imao uvid u validnost rezultata. Na kraju testa, aplikacija pruža mogućnost pamćenja rezultata u više formata (.csv, .txt) na osnovu kojih je moguće dalje manipulisanje dobijenim rezultatima.

IV. Rezultati i diskusija

Uticaj dopiranja i dobijene mikrostrukture na dielektričnu konstantu može se posmatrati i preko zavisnosti dielektrične konstante ε_r od temperature (Sl. 3 i 4, respektivno). U ovom radu ispitivana je i zavisnost dielektrične konstante od temperature u opsegu od 20°C do 170°C i frekvencije u opsegu od 100Hz do 1MHz.

Na osnovu krivih zavisnosti dielektrične konstante od temperature može se videti da najvišu vrednost dielektrične konstante kako na sobnoj tako i na Kirijevoj temperaturi pokazuju uzorci sa koncentracijom aditiva od 0.5at% Nb (ručno merenje, ε_r=4897) i (primena nove metode, ε_r=4763). Najnižu vrednost dielektrične konstante na Kirijevoj temperaturi imaju uzorci sa koncentracijom aditiva (5.0at% Nb) i ona iznosi ε_r=1479 za uzorke ručno merene i ε_r=1445 za uzorke merene primenom nove metode.

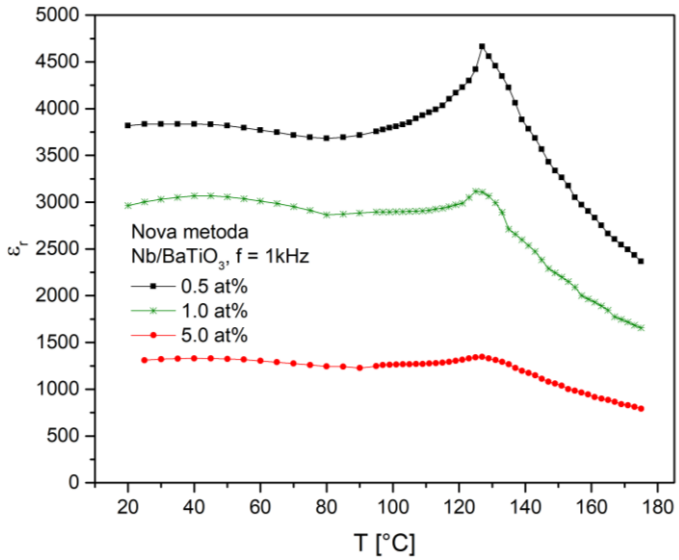

Sl. 3. Zavisnost dielektrične konstante od temperature za različite koncentracije dopanata 0.5 at%, 1.0 at% i 5.0 at% Nb-$BaTiO_3$ merene novom metodom

Kirijeva temperatura (T_C) pri kojoj dolazi do prelaska iz feroelektrične u paraelektričnu oblast iznosi 127°C primenom obe tehnike merenja, čime je potvrđena validnost primenjene nove metode (Sl. 4).

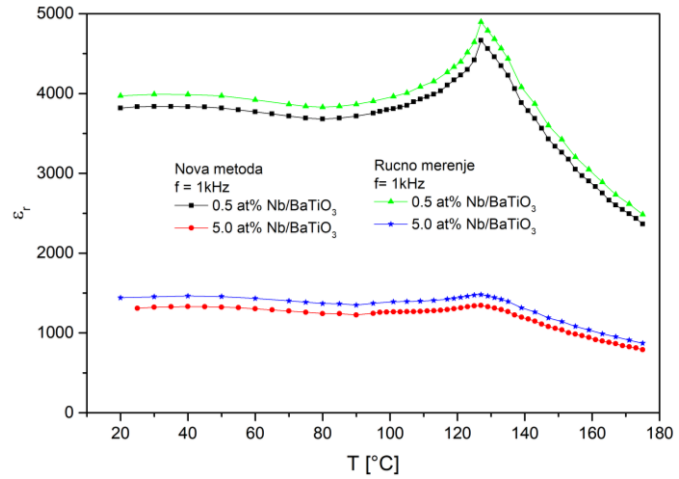

Sl. 4. Zavisnost dielektrične konstante od temperature za različite koncentracije dopanata 0.5 at% Nb i 5.0 at% Nb merene različitim metodama.

Može se primetiti da je učestanost merenja (broj tačaka) ispitivanih uzoraka ručnim merenjem manji od broja tačaka merenih primenom nove metode. Ova činjenica može se ogledati u nekoliko nedostataka koji imaju uticaj na merenje i karakterizaciju ispitivanih uzoraka. Jedan od nedostataka je nemogućnost da se brzo izvrši merenje na zadatoj vrednosti temperature, jer je neophodno izmeriti sve neophodne parametre na različitim frekvencijama.

Pored toga, ručni način merenja utiče i na tačnost izmerenih podataka, s obzirom da se temperatura u peći poveća prilikom merenja svih neophodnih parametara, što utiče na vrednost parametara koji se mere. Ovo se može primetiti na sl. 4, gde su vrednosti za dielektričnu konstantu merene ručno više u odnosu na vrednosti za ε_r izmerene primenom nove metode jer uzorak duže vreme boravi u peći za određeno merenje čime mu se neželjeno poveća temperatura.

Prilikom ispitivanja uzoraka primenom nove metode, radi preciznijeg određivanja Kirijeve temperature, kao i dielektrične konstante vršilo se usitnjavanje koraka merenja. Naime, u opsegu temperature od 30°C do 100°C vršeno je merenje na svakih 5°C, dok se u temperaturnom opsegu od 100°C do 180°C vršilo merenje na svakih 2°C.

Dielektrična konstanta u feroelektricima se menja sa temperaturom, dostiže maksimalnu vrednost na Kirijevoj temperaturi i opada sa daljim povećanjem temperature. Zavisnost dielektrične konstante od temperature u paraelektričnoj oblasti, tj. u oblasti iznad Kirijeve temperature, može se opisati Kiri – Vajsovim zakonom:

$$\varepsilon_r = \frac{C}{T - T_0}. \qquad (1)$$

gde je C – Kirijeva konstanta, T – temperatura, a T_0 – Kiri – Vajsova temperatura.

Fitovanjem zavisnosti recipročne vrednosti dielektrične konstante od temperature, kao što je pokazano na Sl. 5, dobijene su vrednosti Kiri-Vajsove temperature T_0. Kiri–Vajsova temperatura T_0 ima niže vrednosti u odnosu na T_C (T_c=127°C) za sve ispitivane uzorke ispivane primenom obe metode merenja. Najviša vrednost za T_0 dobijena je za uzorake dopirane sa 0.5at% Nb T_0=80.29°C za uzorke merene ručnim merenjem i T_0=81.02°C za uzorke merene primenom nove metode. Najniža vrednost T_0 je dobijena za uzorke dopirane sa 5.0at% Nb T_0=63.29°C za uzorke merene ručnim merenjem i T_0=62.35°C za uzorke merene primenom nove metode.

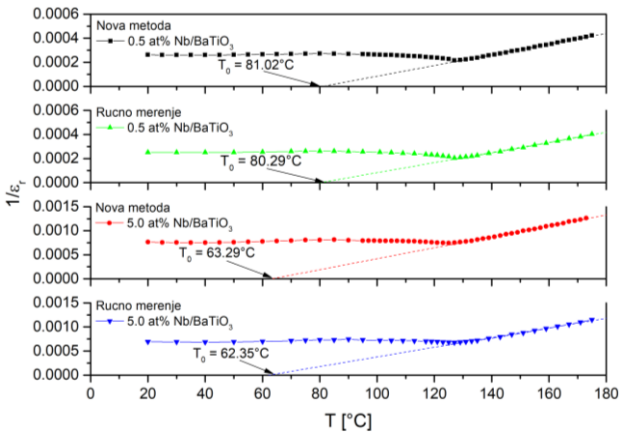

Sl. 5. Vrednosti Kiri-Vajsove temperature T_0 za različite koncentracije dopanata 0.5 at% Nb i 5.0 at% Nb merene različitim metodama

U skaldu sa navedenim nedostatkom ručnog merenja, mogu se primetiti razlike u određivanju Kiri-Vajsove temperature T_0 kada su ispitivani uzorci mereni primenom ručnog merenja i primenom nove metode. Samim tim, prilikom fitovanja veći broj izmerenih tačaka daje preciznije rezultate, što je slučaj sa ispitivanim uzorcima merenih primenom nove metode.

Na osnovu Kiri-Vajsovog zakona izračunate su vrednosti Kirijeve konstante za sve merene uzorke. U Tabeli I date su vrednosti Kirijevog koeficijenta C i Kiri-Vajsove temperature T_0 za sve merene uzorke.

TABELA I
DIELEKTRIČNI PARAMETRI ZA $Nb/BaTiO_3$ KERAMIKU

Metoda	Konc. Nb	C [K] $\cdot 10^5$	T_0 [°C]
Ručno merenje	0.5 at%	1.789	80.29
Nova metoda	0.5 at%	2.652	81.02
Ručno merenje	5.0 at%	0.796	62.35
Nova metoda	5.0 at%	1.045	63.29

Kirijeva konstanta opada sa povećanjem koncentracije aditiva (Tabela I) tako da je najviša vrednost Kirijeve konstante izračunata kod uzoraka sa koncentarcijom aditiva 0.5at% Nb $C=1.78\cdot10^5$ K za uzorke merene ručnim merenjem i $C=2.65\cdot10^5$ K za uzorke merene primenom automatizovane metode, računarom vođenog eksperimenta. Najniža vrednost za Kirijevu konstantu je izmerena za uzorke sa koncentracijom aditiva 5.0at% $C=0.79\cdot10^5$ K za uzorke merene ručnim merenjem i $C=1.04\cdot10^5$ K za uzorke merene primenom automatizovane metode.

Korišćenjem modifikovanog Kiri – Vajsovog zakona:

$$\frac{1}{\varepsilon_r}=\frac{1}{\varepsilon_{r\,\max}}+\frac{(T-T_{\max})^{\gamma}}{C'}. \qquad (2)$$

gde je C' konstanta slična Kirijevoj konstanti određen je kritični eksponent nelinearnosti γ, koji pokazuje odstupanje od linearne zavisnosti dielektrične konstante ε_r od temperature u paraelektričnoj oblasti. Linearnim fitovanjem krivih $ln(1/\varepsilon_r-1/\varepsilon_{rmax})$ u funkciji od $ln(T-T_{max})$ dobijen je γ kao nagib prave za obe tehnike mernja, a grafički prikaz za sve uzorke ilustrovan je na Sl. 6.

Vrednost kritičnog eksponenta nelinearnosti γ kreće se od 1.149 do 1.248 (ručno merenje), odnosno od 1.163 do 1.252 (primena automatizovane metode), što je u skladu sa eksperimentalnim podacima jer je za ove uzorke karakterističan oštar prelaz iz feroelektrične u paraelektričnu oblast što ukazuje na strukturnu faznu promenu.

Najizrazitija promena iz feroelektrične u paraelektričnu oblast zapažena je kod uzoraka dopiranih sa 0.5at% Nb za obe metode merenja (γ=1.149 (ručno merenje) i γ=1.163 (automatizovana metoda)). Najmanja promena primećena je kod uzoraka dopiranih sa 5.0at% Nb za obe metode merenja za koje kritični eksponent γ iznosi 1.248, odnosno 1.252 (ručno merenje i primena automatizovane metode, respektivno).

Slično kao i kod određivanja Kiri-Vajsove temperature T_0 i ovde se potvrđuje činjenica da su prilikom fitovanja većeg broja tačaka (primena nove metode) dobijeni precizniji rezultati.

U skladu sa dobijenim rezultatima primenom automatizovane metode za merenje i karakterizaciju dopirane $BaTiO_3$ keramike, potvrđena je njena validnost prilikom poređenja izmerenih rezultata za iste parametare dobijenih prilikom ručnog merenja. Drugim rečima nije primećeno odstupanje dobijenih rezultata prilikom poređanja. S druge strane, prilikom ispitivanja uzoraka, došlo se do zaključka da su dobijeni precizniji rezultati primenom automatizovane metode. Kao jedna od prednosti se može istaći veći broj merenja, u odnosu na ručno merenje, gde je bilo moguće jedno merenje u toku dana. Naredna prednost predstavlja veći broj tačaka merenja, s obzirom da je moguće birati temperaturni korak, čime je moguće preciznije izvršiti određena fitovanja koja su potrebna za karakterizaciju ispitivanih uzoraka.

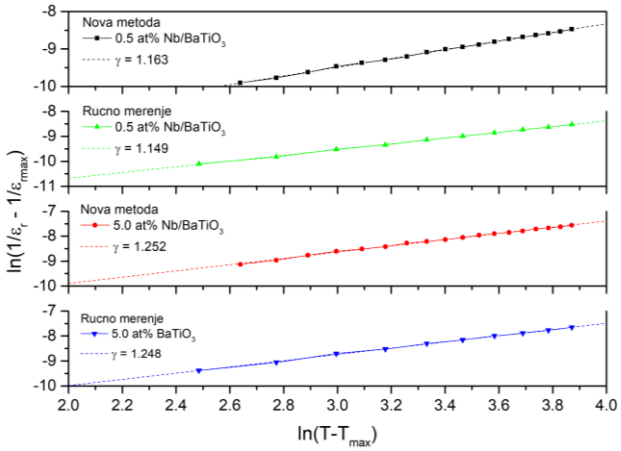

Sl. 6. Zavisnost $\ln(1/\varepsilon_r-1/\varepsilon r_{max})$ od $\ln(T-Tmax)$ za merene uzorke primenom obe metode merenja

V. ZAKLJUČAK

U ovom radu ispitivana su dielektrična svojstva dopirane $Nb/BaTiO_3$ keramike i vršeno poređenje dobijenih rezultata na osnovu dve tehnike merenja. Poređeni su rezultati za ispitivane uzorke merene ručnim merenjem i primenom automatizovane metode. S obzirom da korišćeni LCR metar ne poseduje sopstveni softver, moguće je bilo vršiti ručno merenje uzoraka ili realizovati aplikaciju za virtuelenu instrumentaciju, na osnovu koji bi bila moguća kontrola samog instrumenta.

Prilikom ispitivanja uzoraka primenom ručnog merenja, bilo je nemoguće izmeriti sve neophodne parametre na određenoj temperaturi na različitim frekvencijama u veoma kratkom roku. Razlog tome je što se temperatra u peći povećavala tokom merenja parametara i njihovog zapisivanja, što se odrazilo i na vrednosti za dielektričnu konstantu. Naime, vrednosti za dielektričnu konstantu su više za sve koncentracije dopirane keramike ispitivane ručnim merenjem u odnosu na vrednosti dobijene primenom nove metode.

Pored toga, prednosti nove metode su ponovljivost merenja (kod ručnog merenja samo jedno merenje dnevno), kao i veći broj tačaka mernja, s obzirom da je moguće birati manji razmak između dva merenja.

ZAHVALNICA

Autori se zahvaljuju finansiskoj podršci Ministarstvu prosvete, nauke i tehnološkog razvoja Republike Srbije.

LITERATURA

[1] D.H. Kuo, C.H. Wang, W.P. Tsai, "Donor and Acceptor Cosubstituted $BaTiO_3$ for Nonreducible Multilayer Ceramic Capacitors", Ceram. Int. 32, 2006, pp. 1–5

[2] S.F. Wang, G.O. Dayton: Dielectric Properties of Fine-grained Barium Titanate Based X7R Materials, J. Am. Ceram. Soc., Vol. 82, No. 10, Oct. 1999, pp. 2677 – 2682.

[3] V.Mitic, Z.Nikolic, V.Pavlovic, V. Paunovic, M.Miljkovic, B. Jordovic, Lj. Zivkovic, ″Influence of rare-earth dopants on barium titanate ceramics microstructure and corresponding electrical properties″, *J. Am. Ceram. Soc.* 93 [1] 132-137, 2010 .

[4] V. Paunovic, Lj. Zivkovic, V. Mitic, ″The influence of rare-earth additives (La, Sm and Dy) on the microstructure and dielectric properties of doped BaTiO3 ceramics″, *Sci. Sinter*. Vol.42 pp.69-79, 2010.

[5] Y. Yuan, S.R. Zhang, X.H. Zhou, Effects of Nb_2O_5 doping on the microstructure and the dielectric temperature characteristics of barium titanate ceramics, J. Mater. Sci. 44 (2009) 3751–3757 https://doi.org/10.1007/s10853-009-3502-z.

[6] H. Li, J. Kang, F. Guo, Y. Qu, D. Yang, Effect of the Nb_2O_5 content on electrical properties of lead-free $BaTiO_3$–Bi0.5Na0.5TiO_3 ceramics, Ceram. Int.39 (2013) 7589 – 7593

https://doi.org/10.1016/j.ceramint.2013.03.013.

[7] M. Djordjević, V. Paunović, D. Danković, M. Pejović, "A Method for Automating the Measurement and Characterization of Electrical Materials", The Proceedings of 14th International Conference on Advanced Technologies Systems and Services in Telecommunications, TELSIKS, Niš, Serbia, pp. 219-222, October 2019.

ABSTRACT

This paper describes the comparison of the results obtained manually and by applying a automating method for measuring and characterizing doped $BaTiO_3$ ceramics at different temperatures and frequencies. An LCR meter as a function of temperature and a programmable furnace for testing electrical materials at different temperatures were used to measure and characterize the material parameters. The results obtained by manual control of the LCR meter were measured by manually setting the parameters. The obtained results were compared with the results obtained by applying a new method for automatic control of LCR meters, for which an application was developed. Based on that, it has been shown that the measurement of characteristics can be done without the need for a human. The results compared were obtained on the basis of measurements of samples of doped $BaTiO_3$ ceramics. Based on the measured results, it was noticed that more precise results were obtained when applying the automating method.

Characterization of doped $BaTiO_3$ ceramics using a new method for measuring electrical characteristics

Miloš Đorđević, Miloš Marjanović, Vesna Paunović, Danijel Danković